SAND REPORT

SAND 2004-6229
Unlimited Release
Printed December 2004

Nano Electrode Arrays for In-situ Identification and Quantification of Chemicals in Water

W. G. Yelton
K. B. Pfeifer
D. A. Brevnov
N. J. Gurule
M. J. Kelly
C. I. Ashby

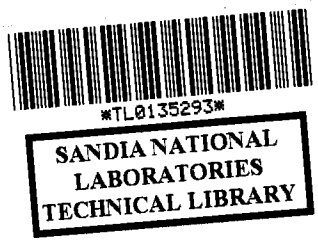

Prepared by
Sandia National Laboratories
Albuquerque, New Mexico 87185 and Livermore, California 94550

Sandia is a multiprogram laboratory operated by Sandia Corporation, a Lockheed Martin Company, for the United States Department of Energy under Contract DE-AC04-94AL85000.

Sandia National Laboratories

Issued by Sandia National Laboratories, operated for the United States Department of Energy by Sandia Corporation.

Available to DOE and DOE contractors from
U.S. Department of Energy
Office of Scientific and Technical Information
P.O. Box 62
Oak Ridge, TN 37831

Telephone: (865)576-8401
Facsimile: (865)576-5728
E-Mail: reports@adonis.osti.gov
Online ordering: http://www.doe.gov/bridge

Available to the public from
U.S. Department of Commerce
National Technical Information Service
5285 Port Royal Rd
Springfield, VA 22161

Telephone: (800)553-6847
Facsimile: (703)605-6900
E-Mail: orders@ntis.fedworld.gov
Online order: http://www.ntis.gov/ordering.htm

SAND 2004-6229
UNLIMITED RELEASE
PRINTED DECEMBER 2004

Nano electrode arrays for In-situ identification and quantification of chemicals in water

Proposal Number 04-1339
Project 38668

W. Graham Yelton, Kent B. Pfeifer, Dmitri A. Brevnov*, Natalia J. Gurule,
Mike J. Kelly, and Carol I. Ashby

Sandia National Laboratories
P.O. Box 5800
Albuquerque, NM 87185-1425

*The University of New Mexico
209 Farris Engineering Center
Albuquerque, NM 87131

1 Abstract

The nano electrode arrays for in-situ identification and quantification of chemicals in water progress in four major directions. 1) We developed and engineering three nanoelectrode array designs which operate in a portable field mode or as distributed sensor network for water systems. 2) To replace the fragile glass electrochemical cells using in the lab, we design and engineered field-ready sampling heads that combine the nanoelectrode arrays with a high-speed potentiostat. 3) To utilize these arrays in a portable system we design and engineered a light weight high-speed potentiostat with pulse widths from 2 μsec. to 100 msec. or greater. 4) Finally, we developed the parameters for an analytical method in low-conductivity solutions for Pb(II) detection, with initial studies for the analysis of As(III) and As(V) analysis in natural water sources.

2 Table of Contents

3 Table of Figures

4 Nano electrode arrays for In-situ identification and quantification of chemicals in water

4.1 Introduction

Electrochemical (EC) analysis is a highly sensitive, chemically selective method for identifying and quantifying many different chemicals in water. Sub-part-per-billion sensitivity levels are achievable for many EPA-regulated chemicals and for many of the chemicals proposed for future regulation. Unfortunately, EC analysis has historically required that field samples be transported to an analytical laboratory where additional laboratory chemicals must be added to samples before an EC analysis can be performed with bench-scale equipment. This requires skilled laboratory technicians and causes unacceptable time delays when immediate information about the safety of a particular water source is needed. Furthermore, sample degradation may occur during sample transport to the laboratory and thereby causing further uncertainty in the analytical results. Conventional off-site laboratory analysis is also too costly if comprehensive, continuous monitoring of the health of a water distribution system is desired.

The mandatory addition of chemicals for currently available electrodes to work well with many water samples is a key limiting factor preventing on-site, real-time measurements and distributed unmanned operation. The overarching goal of this project has been the development of a new type of electrode system that overcomes the limitations of current electrode designs and can enable both portable, battery-powered field testing and continuous remote system monitoring. To reach this goal, integrated arrays of nanoelectrode elements and portable control electronics for electrochemical measurements using the arrays have been developed.

Due to their size, the working electrodes most often used in electroanalysis today require the addition of an electrolyte to the solution to adjust the conductivity, ionic strength, and/or pH of the solution before an accurate EC analysis can be made. Further, the incorporation of "microelectrodes" in analytical methods is severely hampered by the small faradaic currents (i.e., small analytical signals) typical for these electrodes, and they too require supporting electrolytes for proper operation. For example, a 1-micron-diameter working electrode typically requires that the supporting electrolyte solution be added to achieve a minimum resistivity of 80-100 Ω-cm. This mandates the presence of a trained technician to properly adjust solution concentrations. Reduction of the electrode dimension from the microscale to the nanoscale removes these resistivity limitations, enabling unattended operation or direct measurements by simple immersion in a water source without any electrolyte addition. For example, an ensemble of 40-nm-radius electrodes with an areal density of $1x10^{11}$ electrodes/cm^2 can produce an easily detectable current density of 5μA/cm^2 from a 1-ppb analyte concentration even in solutions with resistivities as high as 10^6Ω-cm, typical of DI water.

A major advantage of employing an array of nanoelectrode ensembles is the selectivity for high priority analytes that can be realized by chemical modification of the nanoelectrode surfaces. Individual nanoelectrode elements within an array can be chemically treated to provide a working electrode surface with enhanced specificity and

sensitivity for priority analytes. Further selectivity in the analysis, including discrimination from interfering species in the water, can be derived from the fact that the thermodynamics and kinetics of the heterogeneous electron transfer reaction (i.e., the reduction or oxidation of the analyte) are different from those of many interferents. The deposition of gold surfaces in the nanoelectrode arrays provides a working electrode surface that is extremely well-suited to the analysis of As(III), As(V), Hg(II), Hg_xCl_y (so-

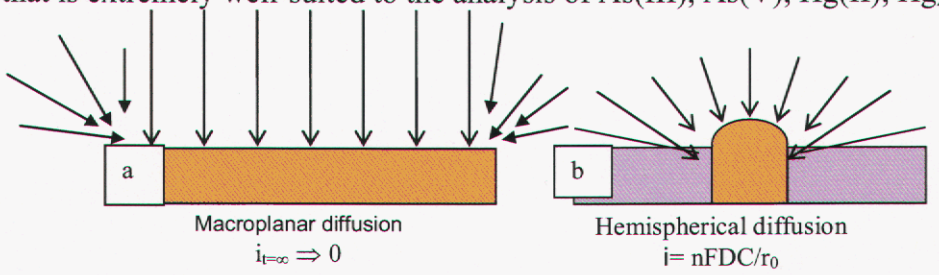

Figure 4.1: Schematic of macro electrode with planar diffusion flux with small edge diffusion (a) and nano electrode with hemispherical diffusion flux mostly from edge diffusion (b).

called "reactive mercury), Cr(III), Cr(VI), Pb(II) and other priority analytes. Chemical modification of the nanoelectrode surfaces with polymeric coatings can increase the selectivity and sensitivity of some analyses via preferential adsorption of the analyte in the coating. For example, modification of carbon electrodes with amide-functionalized humic acids has been reported to produce a highly selective working electrode that can analyze mercury in river water at concentrations as low as 10 ppb.

4.2 Nano-Electrodes

For a single electrode: The nano-scaled electrode for electrochemical sensors has the greatest influence over any other geometry. 1) It extends the range of measurable current densities due to the fact that limiting current densities are inversely proportional to the radius of the electrode and 2) the resistively is proportional to the radius.

Generally speaking, the sensitivity of an electrochemical electrode (sensor) is proportional to the diffusion-limited current density i_d as a function of applied potential.

$$i_d = \frac{nFDC}{\delta} \qquad (4.1)$$
$$such \quad that \quad \delta = (\pi Dt)^{1/2}$$

Here n represents the number of electron transferred in the electrochemical reaction, F is Faraday's constant, D is the diffusion coefficient of the electroactive species, C is the bulk concentration of the species in the solution far from the electrode, and δ is the Nernst diffusion layer thickness that develops around the electrode when current flows.

Thus, the diffusion-limited current density i_d decreases with the square of time as the Nernst diffusion layer thickness develops. A lot is gain with fast transients (measurements) which has the same affect as increasing the rate of mass transport by more efficient agitation. But as the diameter of the electrode decrease as compare to a planar case (Figure 4.1) the edge-effects of current density become dominating and the

diffusion flux of electroactive species for micro-disks diffusion-current density becomes independent of time.

$$i_d = \frac{nFDC}{r} \tag{4.2}$$

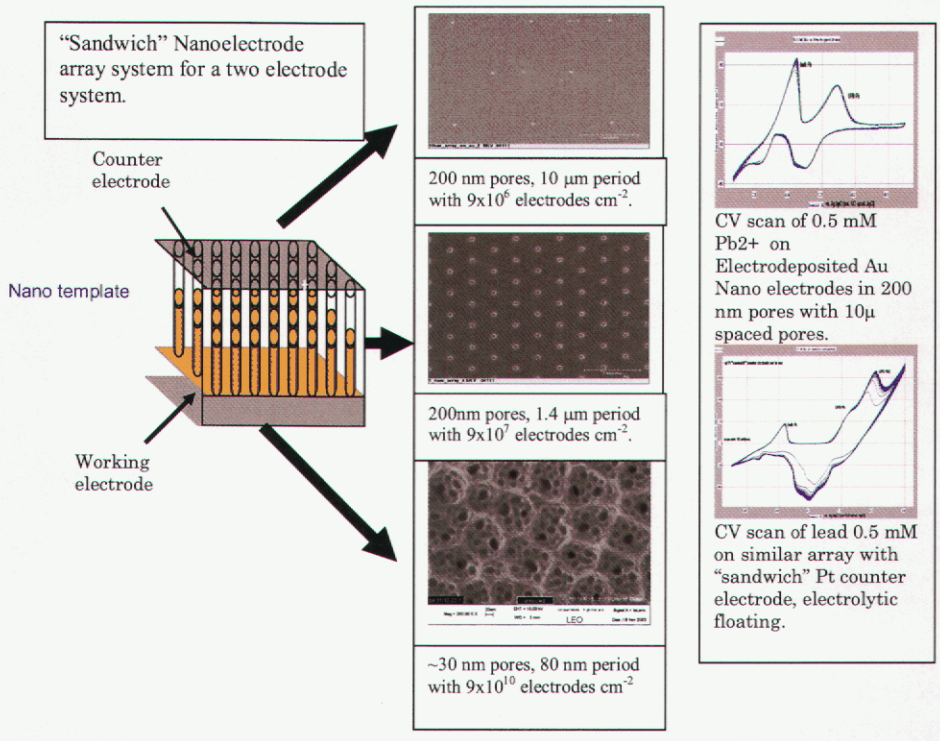

Figure 4.2: The three fundamental design concepts involved using PMMA as lithography pattern arrays or the anodized aluminum oxide (AAO) films as templates for nanoelectrodes arrays. Typical cyclic voltammetry scans using nanoelectrode

Example: The diffusion-current density obtained from a nanocarbon, where r = 400 Å is capably of yielding an incredible 5 A/cm^2. For an electroactive concentration of 10 mM, where n=2, and D=1x10^{-5}. Such limiting current densities cannot be reached at steady state by either rotating disk electrodes operating at 10^4 rpm or by any other method. The advantage of having a very large limiting current density at steady state, not affected by solution flow, is in the analysis of trace elements. For an electrode diameter of 400 Å, we can obtain an i_d = 5μA/cm^2, for a concentration of 0.001 ppm (base on MW= 100) which should be easily detectable with present instrumentation.

Two major disadvantages to microelectrodes: 1) since a single electrode is small, the *total* current flowing in the circuit is very small and extremely difficult to measure. Example: For an electrodes with D=400 Å, the total surface area is 1.3 X 10^{-11}, for a 1mA/cm^2 current density, the total current is 10^{-14} A. This is clearly not possible to measure with any degree of accuracy. 2) Another disadvantage is the extremely high Volume to Surface Area ratio V/A, for these electrodes and the effects from impurities accumulating

on the surface during measurement. For a V/A ratio of 10^8 cm, a conservative measurement for an ultramicro-electrode, the level of purity needed to prevent fouling is not achievable.

4.3 Nanoelectrode Arrays or Ensembles

One solution around these problems, and still retain the advantages of the nano electrode is to build ordered arrays of 10,000's if not 1,000,000's electrodes or use films with natural accruing nano size ensembles to serve as electrode templates. The challenge of designing such an array is the compromise between making the ratio of the electrode diameter and the length between electrodes, $(d/L)^2$ not too large or too small. If the ratio is too large, the diffusion fields of the individual electrodes will overlap resulting in a single planar electrode effect. Consequently, if the ratio is too small, the total active surface area of the array is low making total current flow difficult to measure.

In terms of the Nernst diffusion layer thickness and the radius of the electrodes, and the distance between electrodes, we have control over the i_d by taking advantage of varying transient periods or varying the design and geometry of the array.

For example:

Case 1 when $\delta/r \leq 0.3$

Here the system is in the range of semi-infinite linear diffusion near each nanoelectrode, where current density is time dependent.

$$i_d = \frac{nFDC}{(\pi Dt)^{1/2}}\left[\frac{r}{L}\right]^2 \tag{4.3}$$

Case 2 when $\delta/r \geq 3$ but $\delta/L \leq 0.3$

Under these conditions, the diffusion field around each electrode is spherical and the overlap between the diffusion fields of neighboring electrodes is negligible, current density is then independent of time.

$$i_d = \frac{nFDC}{r}\left[\frac{r}{L}\right]^2 \tag{4.4}$$

Case 3 when $\delta/L \geq 3$

In this regime, complete overlap between the diffusion fields of individual electrodes are predominate, and the array appears as one large planer electrode where current density is again time dependent with the largest signals appearing only from fast transients.

$$i_d = \frac{nFDC}{(\pi Dt)^{1/2}} \tag{4.5}$$

4.4 Array Fabrication

Nano electrodes and templates provide the use of functionalized nanoelectrodes as sensor-array systems for rapid, non-contaminating field analysis. An array of suitably functionalized nanoelectrodes could be incorporated into a small, integrated sensor system that can identify many species rapidly and simultaneously under field conditions without chemical addition with signal to noise ratios (S/N) up to 10^3-fold greater than conventional electrodes.

The SEM microphotographs in Figure 4.2 are templates with 200 nm pores space 10 and 1.4 microns respectively. These first two microphotographs are copper substrates with evaporated nickel and gold followed by a layer of Poly methyl methacrylate (PMMA) photoresist. The holes are generated by laser lithography to generate this pattern of pores. To make a "sandwich" two electrode nanosystem, a counter electrode of platinum is deposited on top of the PMMA (Figure 4.2). Then any metal connections between the Au and Pt are cleared using a pulse of high current. After which periodic pulse electrodeposited processes (pore filling) are used to create a layer of nano electrodes using either Au or Ag. Arrays spaced on a 10 micron period yield ~9 million electrodes /cm2. Ones spaced 1.4 microns apart yield ~90 million electrodes /cm^2. The third electrode design is the anodized aluminum templates (Figure 4.2) with randomly deposited gold electrodes, these are 30-50 nm diameters spaced any where between 50 - 500 nm from each other.

5 Anodic aluminum oxide (AAO) as a template to fabrication arrays of nano-electrodes

5.1 Introduction

The Anodic aluminum axide (AAO) array is a self-ordered nano-structure, which is attractive for design of the array of nano-electrodes. The technological utility of AAO results from three main characteristics: the hexagonal pore arrangement, high pore density, and a very high aspect ratio (the ratio between the pore length and pore diameter). In this report, we provide a summary of our research efforts for the period since September 2003 until September 2004. First, we report on obtaining a better understanding of anodization of aluminum and etching of aluminum oxide. Second, we describe the formation of the secondary pore structure. Third, we report on our attempts to perform electrodeposition of gold and silver in the pores of AAO.

5.2 Anodization of aluminum and etching of aluminum oxide

The procedure to prepare AAO arrays is well established.[1,2] In spite of the simplicity of the fabrication method, the processes that take place during porous-type anodization in acidic electrolytes are complex. The AAO array consists of three distinct layers: aluminum metal, a thin barrier oxide layer, and a relatively thick porous oxide layer. The electrochemical reaction (oxidation of aluminum to produce Al_2O_3), takes place at the aluminum metal / barrier aluminum oxide interface. At applied voltages of 10-70 V, the rate of anodization is limited by the rate of migration of ions through the layer of barrier aluminum oxide. The thickness of this layer depends linearly upon the anodization voltage. During anodization at a constant voltage (DC), the thickness of the barrier

aluminum oxide remains constant, because the rate of alumina dissolution on the electrolyte side is equal to the rate of alumina production on the metal side (steady state AAO array formation).[2] Complex anodization processes can be studied by non-destructive electrochemical and optical methods such as electrochemical impedance spectroscopy (EIS). EIS can be used to determine the thickness of barrier aluminum oxide.[3, 4] The simplest equivalent circuit, which describes the aluminum/alumina/electrolyte system at an open circuit potential (OCP), includes the uncompensated resistance and a parallel combination of the barrier aluminum oxide capacitance and a resistor.[3] High conductivity of acidic electrolyte causes a short-circuiting effect in the porous oxide layer.

It has been previously demonstrated that a two-step procedure is necessary for fabrication of highly ordered AAO arrays.[5,6] The first step involves growth and sequential etching (dissolution) of alumina. The second step (second anodization) leads to formation of highly ordered AAO arrays. In spite of the many applications of the two-step procedure, there is some variability in experimental conditions used for anodization and etching of

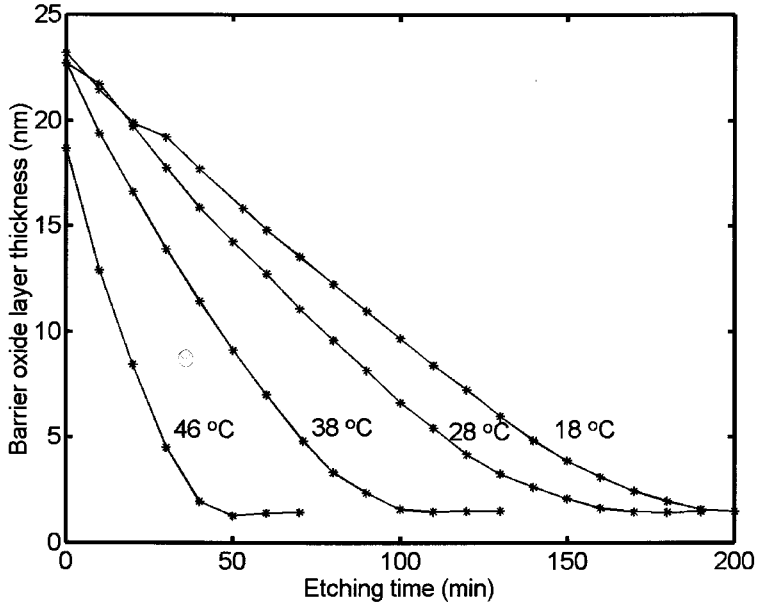

Figure 5.1: The thickness of the barrier aluminum oxide during etching in a mixture of phosphoric and chromic acids.

alumina. For example, with the similar anodization times at the first step, etching times vary among different recipes. Most likely this variability results from inadequate estimates of how fast anodization of aluminum and etching of alumina proceed. Accurate information about these rates can be obtained by applying EIS for non-destructive monitoring of growth and dissolution of barrier oxide layers.

We employ EIS to monitor dissolution of barrier aluminum oxide during the two-step procedure.[7] To etch alumina layers formed after the first anodization step in a solution of 3% w/v oxalic acid at 30 V for 20 minutes, the electrochemical cell was rinsed with cold water, filled with a solution of mixed acid and maintained at chosen temperatures (18 °C, 28 °C, 38 °C, and 46 °C). The dissolution of barrier aluminum oxide was followed by EIS

measurements. The total cell impedance can be modeled as two parallel combinations of a constant phase element (CPE) and a resistor (R) connected in series with each other and the cell uncompensated resistance. The CPE is frequently used instead of a pure capacitance to describe interfacial dielectric properties. One of two parallel (R_1 CPE_1) combinations is readily attributed to barrier aluminum oxide. In this case, CPE_1 describes the dielectric properties of barrier aluminum oxide and R_1 describes the resistance to ion migration through this layer. The other (R_2 CPE_2) combination is likely to originate from the barrier aluminum oxide / aluminum interface. The thickness of the barrier oxide layer was calculated assuming that the dielectric constant of aluminum oxide is 8.6. Because of the slow rate of dissolution, the layer of barrier aluminum oxide was assumed to be quasi-stable over the time period of EIS measurements (about 3 minutes). The EIS scan was repeated every 10 minutes. Figure 5.1 shows that the thickness of barrier aluminum oxide decreases linearly with time at a constant temperature. A constant dissolution rate of alumina is a consequence of the constant electrode area exposed to the etching electrolyte. From the analysis of the Figure 5.1, we conclude that at a constant temperature the dissolution of barrier aluminum oxide starts immediately after exposure of the anodized aluminum sample to the solution of mixed acid and proceeds with an almost constant rate until the thickness of barrier aluminum oxide becomes constant.

In summary, EIS experiments are of extremely practical utility for monitoring the dissolution barrier aluminum oxide dissolution and, as a result, determination of the necessary duration of the etching process. For example, at 38 °C the dissolution rate is about 0.3 nm/min (Figure 5.1). Therefore, the anodized sample has to be subjected to the etching solution for about 2 hours in order to dissolve the barrier oxide layer formed after anodization at 30 V. Knowing the activation energy (42 kJ/mole) allows for determination of an etching time at temperatures higher than reported here. For example, at 60 °C it would take about 35 minutes to dissolve the barrier layer formed under the same anodization conditions (30 V, 3% w/v oxalic acid).

5.3 Development of the secondary pore structure during anodization of aluminum

The inherent constraint of using the porous aluminum oxide layer, as a template for electrode development, is the ratio between the inter-pore distance and pore diameter. To utilize the benefits of an array of ultra-micro electrodes (UME's), the ratio must be such that diffusion profiles from individual electrodes do not overlap each other. If the pores are too closely packed together, the resulting diffusion profiles from each electrode will overlap and each electrode will no longer act independently. As a result, the faradaic current collected with an array of UME's mimics one observed with a planar electrode.

A new technique for controlling the ratio between the inter-pore distance and pore diameter must be developed in order to produce an anodized template with pore arrangement optimal for use as an array of UME's. The objective of this research project is to develop a method to maximize the ratio between the inter-pore distances and pore diameters. We suggest that this objective can be achieved by utilizing a hierarchy of pores, which can be developed on a sample of anodized aluminum oxide. By anodizing at room temperature, two generations of pores can be grown. The first generation or the primary pores, demonstrate both pore diameters and inter-pore distances similar to ones

found in the literature. The second generation or secondary pores are a smaller sub set of pores that develop at the bottom of the larger, primary pores. The diameter of the secondary pores is approximately 20% of the diameter of the primary pores. The growth of these secondary pores provides a new method of increasing the ratio between the inter-pore distance and pore diameter. This new arrangement would provide a template whose spacing is ideal for use as an array of UME's.

During typical anodization conditions, the ratio between inter pore distance and pore diameter is about 2-3. We determined that a higher ratio can be obtained by generating a secondary pore structure. This structure was fabricated under the following experimental conditions. Anodization was performed at 22-23°C and in a 3 % w/v solution of oxalic acid. This step was followed by etching for 40 minutes at 70°C in a mixture of 0.4 M phosphoric and 0.3 M chromic acids. Anodization was then repeated under the same conditions as the first step for a time of 3 hours.

We observed that two-step anodizations performed at room temperature produced two distinct sets of pores. The first set of pores is hexagonally arranged with inter pore distances linearly proportional to the applied voltage. These pores develop during the first step of the anodization process. The smaller, secondary sets of pores only began to develop during the second step of the anodization and do not depend upon applied voltage. The smaller, secondary pores are a function of the length of time the second step of anodization is allowed to proceed. This progression of primary and secondary pore growth is illustrated in **Figure 5.2** (a,b,c,d) and **Figure 5.3** (a,b,c.d). The top views are demonstrated in **Figure 5.2** (a,c) and **Figure 5.3** (a,c), while the cross-sections are shown in **Figure 5.3** (b,d) and **Figure 5.3** (b,d).

Figure 5.2 (a,b) shows the state of the surface after completion of the first anodization for 30 minutes. At this point, only the grain boundary of aluminum is visible. **Figure 5.2** (c,d) demonstrates that both the porous and barrier oxide layers are completely removed after etching. The thickness of barrier oxide layer left on the surface closely corresponds to the thickness of the native aluminum oxide. **Figure 5.3** (a,b) indicates that the secondary pore development only occurs after the second step of anodization for 30 minutes. **Figure 5.3** (c,d) demonstrates full development of the secondary pores. The measurements of pores diameters indicate that the diameter of the vertical pores in **Figure 5.3**b is the same as the diameter of the smaller pores in **Figure 5.3**d. Also, the diameter of the larger pores in **Figure 5.3**c is equal to the width of the larger, scalloped portion of **Figure 5.3**d that extends down 30-40 nm from the surface.

The porous oxide layers obtained from anodizations at room temperature are different from ones obtained during anodizations at 0°C. At room temperature the larger, primary pores increase in diameter and inter pore distance due to increased applied voltage similarly to anodizations 0°C. However, at room temperature, the ratio of the inter pore distance to pore diameters is significantly higher than one obtained at 0°C. This is the result of the growth of the smaller secondary pores. While the inter pore distance is approximately the same at 0°C and 22°C, the development of the secondary pores allow for highly increased pore spacing. This increased inter pore spacing is demonstrated in **Figure 5.2** and **Figure 5.3**.

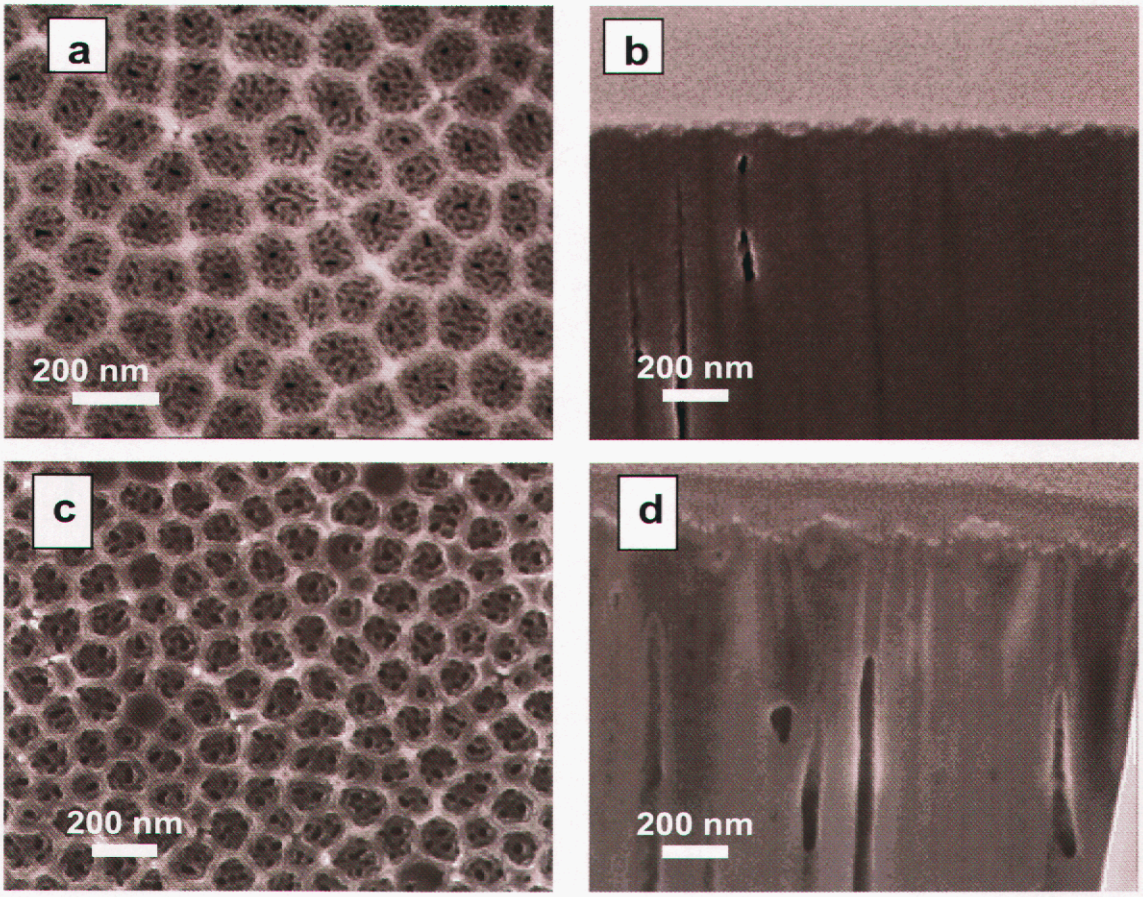

Figure 5.2: top view showing initiation of secondary pore development after 30 minutes into second anodization, (b) cross section after 30 minutes into second anodization, (c) top view after the second anodization for 3 hours, (d) cross section after the second anodization for 3 hours.

Cross sectional micrographs show that the smaller, secondary pores are true and distinct pores, which are separated from the larger primary pores. According to these cross sections, the primary pores are 30-40 nm deep with the secondary pores comprising the rest of the pore depth in the sample. Therefore, it is expected that electro deposition of metals into the porous anodized films will occur inside the secondary pores. Development of secondary pores at room temperature allows ratios of inter pore distance to pore diameter of 4-6 to be achieved. Pore spacing of this magnitude separates neighboring pores far enough to avoid the overlap of diffusion profiles generated at each individual nanoelectrode. In conclusion, the secondary pore structure was observed for the first time and may be exploited for design of UME arrays.

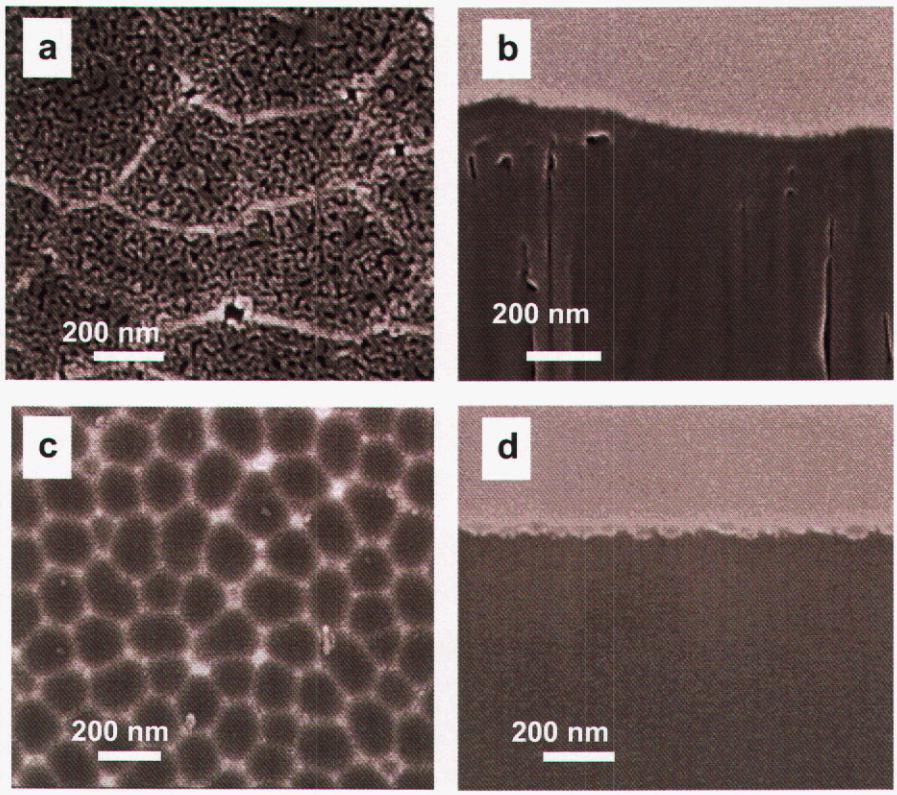

Figure 5.3: (a) Top view of the surface after completion of the first anodization for 30 minutes, (b) cross section of surface after 30 minutes of anodization, (c) top view after etching, (d) Cross section after etching.

5.4 Electrodeposition of gold and silver into pores of AAO

The primary obstacle for electrodeposition of electrically conductive materials in the AAO pores is the presence of the thick layer of barrier aluminum oxide. In order to overcome this problem we implemented the following approach, which included four basic steps. First, we utilize the two-step anodization method to fabrication the ordered AAO arrays. Second, we dramatically reduce the thickness of the barrier oxide, while keeping the porous oxide layer intact. The thinning of the barrier oxide is accomplished with the voltage reduction method (VRM). Third, we perform ac electrodeposition of gold inside the AAO pores.

The main requirement for the procedure described above is VRM, which was originally utilized for complete detachment of the AAO membrane from the underlying aluminum support.[8] This method involves the step-wise voltage reduction from a value specified during the AAO array growth (e.g. 40 V) to a smaller value (e.g. 1 V).[9] As a result, the thickness of barrier aluminum oxide, which is linearly proportional to the applied voltage, decreases. **Table 5.1** shows the capacitance and thickness of the barrier aluminum oxide during the fabrication procedure. The analysis of EIS data suggests that VRM effectively reduces the thickness of barrier aluminum oxide. Supplementary information about the implementation of VRM comes from the evaluation of the cross-sectional micrographs

obtained for samples subjected to anodization and VRM. As shown in **Figure 5.4**, the layer of porous aluminum oxide remains intact. The pores are cylindrical in the middle of the layer. At the same time, pores become conical as they approach the interface between aluminum and barrier aluminum oxide (at the bottom of the micrograph). This result is expected from previously published data on the implementation of VRM.[8] The conical structure of pores supports our conclusion that VRM effectively makes the layer of barrier aluminum oxide thin.

Table 5.1

Step	Capacitance ($\mu F/cm^2$)	Thickness (nm)
First anodization (60V)	0.13	57
First etch (180 min)	4.4	1.7
Second anodization (60 V)	0.13	57
VRM	5.0	1.5

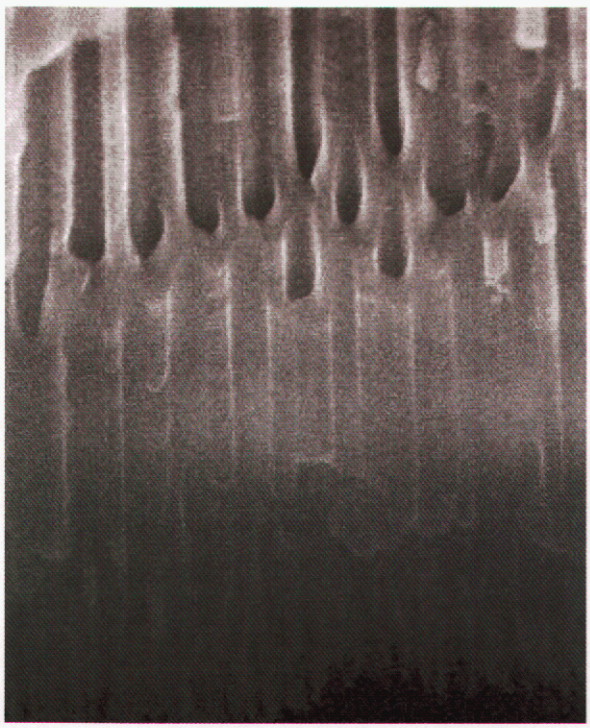

Figure 5.4. The cross sectional micrograph, the porous and barrier oxide layer after VRM.

Following VRM, we typically perform electrodeposition with ac voltage with frequency of 100 Hz and amplitude of 1 V and DC bias of -1.4 -1.8 (vs. Ag/AgCl) depending upon the thickness of barrier aluminum oxide. The commercial gold platting solution (Oromerse, Part B) is used in all experiments. The concentration of gold sulfite is 10 mM and concentration of sodium sulfite was 1.0 M. Figure 5.5 shows that the state of AAO array after electrodepostion. The AAO template can be seen at the background. Dots on the surface represent gold nanorodes deposited in the pores of AAO.

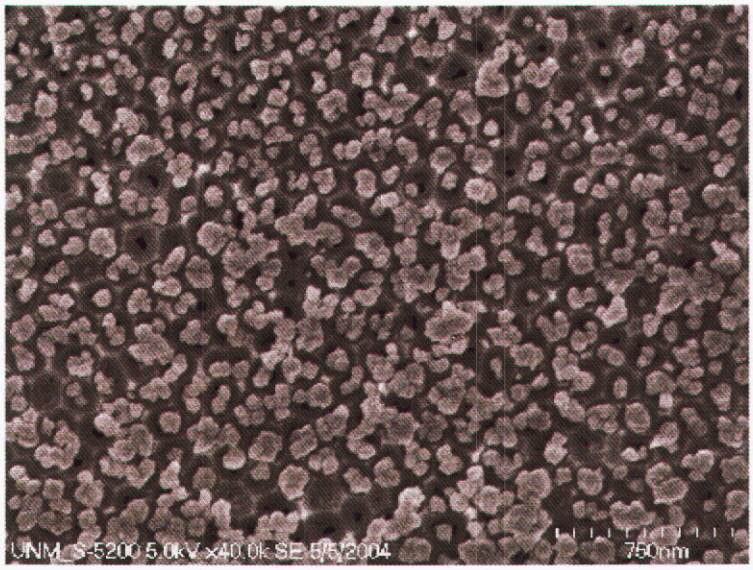

Figure 5.5. Micrograph of gold rods deposited by using AAO as a template.

Regardless of some feasibility of the method described in this section to deposit gold inside the pores of AAO, it is necessary to stress that ac electrodeposition has not been successful for all samples. Pour reproducibility may result from variations in the thickness of barrier aluminum oxide. It is believed that under our experimental conditions VRM results in a gradient of the thickness along the surface. In other words, the thickness of barrier aluminum oxide is different from one point to another. Obviously, electrodeposition takes place in only those areas, which have a thin layer of barrier aluminum oxide.

A better control of the quality of the gold rods deposited inside AAO pores can be achieved with an alternative method. This method utilizes the vacuum deposition of a thin layer of platinum on titanium-coated silicon wafers and subsequent deposition of a thick layer of aluminum (more than 3 microns). In this case, anodization and pore formation proceeds until all aluminum down to the platinum layer is consumed and converted to porous alumina. The exposed platinum at the pore bottoms was used as the working electrode for electrodeposition. This method is believed to be better suitable for fabrication of an array of nano-electrodes.

5.5 References

1. J. W. Diggle, T.G. Downie, C. W. Goulding, Chem. Rev. 69 (1969) 365.
2. A. Despic, V. Parkhutik, in Modern Aspects of Electrochemistry, Vol. 23, Bokris, J. O'M., White, R. E., Conway, B.E., Eds.; pp. 401-493, Plenum Press: New York, (1989).
3. T. P. Hoar, G. C. Wood, Electrochim. Acta 7 (1962) 333.
4. J. De Laet, J. Scheers, H. Terryn, J. Vereecken, Electrochim. Acta 38 (1993) 2103.
5. H. Masuda, M. Satoh, Jpn. J. Appl. Phys. 35 (1996) L126.
6. F. Li, L. Zhang, R. M. Metzger, Chem. Mater. 10 (1998) 2470.
7. D. A. Brevnov, G. V. Rama Rao, G. P. Lopez, P. B. Atanassov, Electrochim. Acta 49 (2004) 2487.
8. R. C. Furneaux, W. R. Rigby, A. P. Davidson, Nature 337 (1989) 147.
9. D. A. Brevnov, M. J. Barela, M. J. Brook, G. P. Lopez, P. B. Atanassov, J. Electrochem. Soc., 151 (2004) B484.

6 Development and use of the nano arrays for trace analyses

6.1 Cyclic Voltammetry

Cyclic Voltammetry (CV) serves as a useful tool to determine the stability of the working electrode as well as the location of the specific peaks. We tested the low density nanoelectrode arrays in a dilute solution of 1.0 mM Potassium Ferricyanide [K3Fe(CN)6]

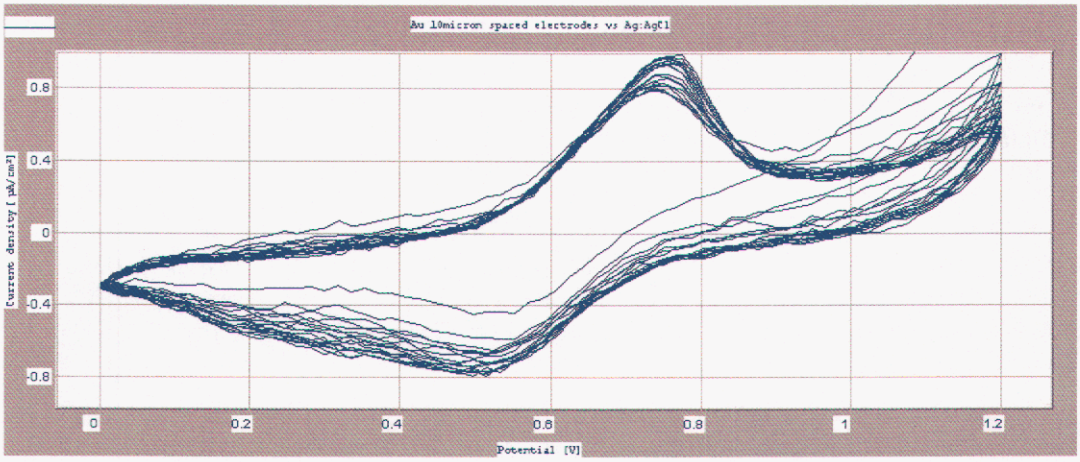

Figure 6.1: Cyclic voltammetry of the redox peaks for 1.0 mM Fe^{2+}/Fe^{3+} in DI water using 200 nm diameter gold nanoelectrodes spaced 10 µm apart. Scan rate 25 mV/sec vs. Ag:AgCl (sat. KCl w/sat. AgCl).

in DI water. Ferricyanide was chosen because of the well known position of the oxidation and reduction peaks. Figure 3.1 is a rough graph of the cyclic votammety from a 200 nm diameter gold nano electrode array with 10 µm spacing between electrodes. The unit area of all graphs is based on unity. A three electrode system in our standard lab cell without agitation under constant temperature was used during the analyses.

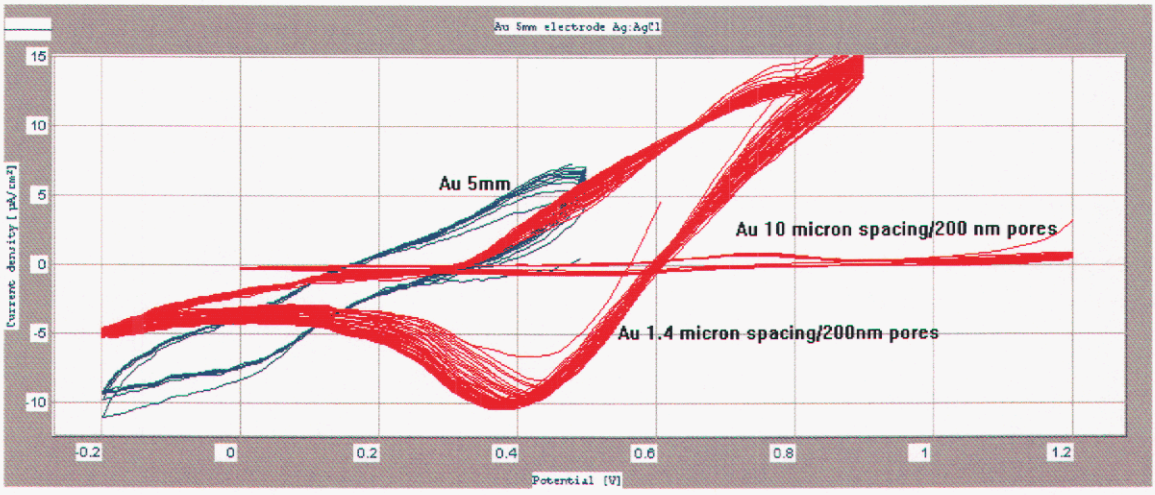

Figure 6.2: Overlay of three CV scans from the same cell using DI water with 1-mM Potassium Ferricyanide [K3Fe(CN)6] comparing working electrodes. The Au 5 mm tip is a commercial working electrode under dynamic ohmic drop compensation. Nanoelectrodes of Au with 10 and 1.4 µm-spacing without ohmic drop compensation are also displayed.

The CV graph in Figure 6.1 is rough and the peaks are shifted to the right by ~200 mV as compared to a standard scans in solutions with conductive salts using a macro electrode of the same geometric area. Remember, the insulating layer on top with the patterned pores (electrodes) is PMMA. As this material is exposed to solution, the polymer swells yielding a rough signal. Interestingly, Figure 6.1 yields a strong oxidation peak (~+750 mV) in solution without the addition of a conducting salt.

The CV scans in Figure 6.2 are the overlay from three working electrodes. The Au nanoelectrode array with 10 µm spacing is the same scans displayed in Figure 6.1. Because of the scale of the response, this scans appears featureless and collapsed. As the number of electrodes in the array increase, the response signal increases. The CV scan of the array with 1.4 µm-spacing is much larger than the array with 10 µm-spacing even though the electrode size and material are the same.

The Chrono Amperometry experiment in Figure 6.3 demonstrates the stability of the arrays compared to the commercial electrode in low conductive solutions. Both arrays have lower signal to noise levels at open (near-open) circuit potentials. Once a pulse is

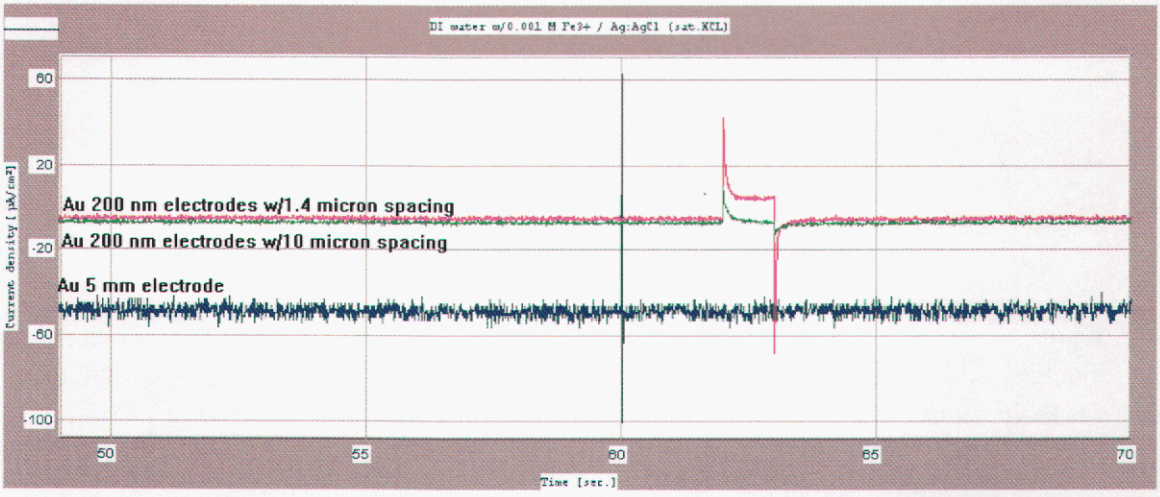

Figure 6.3: Chrono Amperometry in DI water with 1.0 mM Fe^{3+}, pulses are 100 msec. periods for 5 mm gold electrode with pulse potential at +200 mV vs Ag:AgCl (sat. KCL), and an off-pulse potential at 0 mV. Nano electrode array pulsed at +400 mV, off pulse at OCP vs. Ag:AgCl (sat. KCL).

generated, the signal stabilized to a steady state after the charging transit. At +200 mV, the commercial electrode displayed a large transit that quickly decays into the baseline.

6.2 Ag Electrode Affinity for Trace Lead

This experiment was undertaken to check all applicable curves for 0.5 mM Pb^{2+} concentration. The electrodes used were 5 mm diameter Ag working electrode coupled with an Ag quasi-reference electrode rod. A supporting electrolyte was necessary for the lab cell because the ohmic drop was too large. The supporting electrolyte consist of 10mM KCl and 10mM HNO_3. The experimental parameters were as follows:

- Pot. Interactive CV Potential was run at 0mV to -1000mV. The scan rate was 25mV per second.

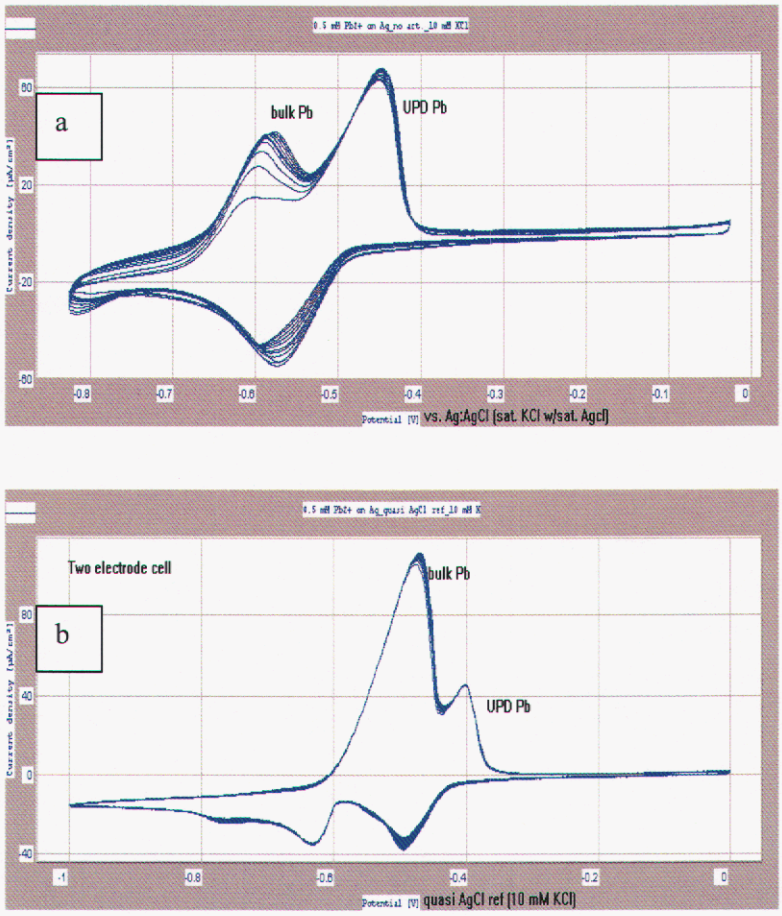

Figure 6.4: CV of 0.5 mM Pb^{2+} in 10mM KCl using a three-electrode system (a) and a non-activated two-electrode system using a silver rod as a quasi-reference counter electrode (b) with an activated 5 mm diameter commercial Ag electrode, scan rate 25 mV/sec.

- Open circuit potential was run once at the beginning of the sequence with duration of 4minutes and a measuring period of 0.2 second. The drift threshold was 1 mV per minute. All applicable peaks were present at the end of this experiment. Key results are listed:
- CV of Pb^{2+} on Ag electrodes gives strong UPD peak even under fowled conditions.
- Strong peak for conditioned electrodes using a quasi-ref/counter electrode system.

The results of the CV voltammetry (Figure 6.2) for either a non-activated (fouled, Figure 6.2a) electrode or a well activated (Figure 6.2b) electrode yield strong peaks for both the bulk lead peak and the under potential deposition (UPD) peaks. The active working electrode gives a stronger CV that is slightly shifted to a more positive potential. Silver will sever well as a working material for the detection of soluble lead in water.

6.3 Nano Au Electrode Affinity for Trace Lead

Under similar solution conditions used in the silver electrode experiments, CV work was performed using gold working electrodes. The result of Figure 6.4a is a CV scans using a 5 mm diameter gold commercial electrode with electrode plated gold on top of the activated gold surface. This CV help simule the effects of electroplated gold in nano pores. Although the peaks appear strong, typically gold yields a second, weaker UPD peak around -50 mV verse Ag:AgCl. The presents of a second peak positive of the first looks more typical of a silver peak. The silver is possible, because of the silver reference electrode leaks at 8 µL/hr. We have seen this peak when the reference electrode sits in the working solution all day.

This experiment is repeated using a nanoelectrode array with 200 nm pores using a gold substrate spaced 10µm from each electrode. The results (Figure 6.4b) are similar to electrode plated commercial electrode, except for absents of potential peaks more positive than the bulk and UPD peaks. Using the soft polymer for the insulating layer presented the following concerns:

- Mechanical polishing was not possible, but fresh electrodeposition yielded strong signals and good peak separation.

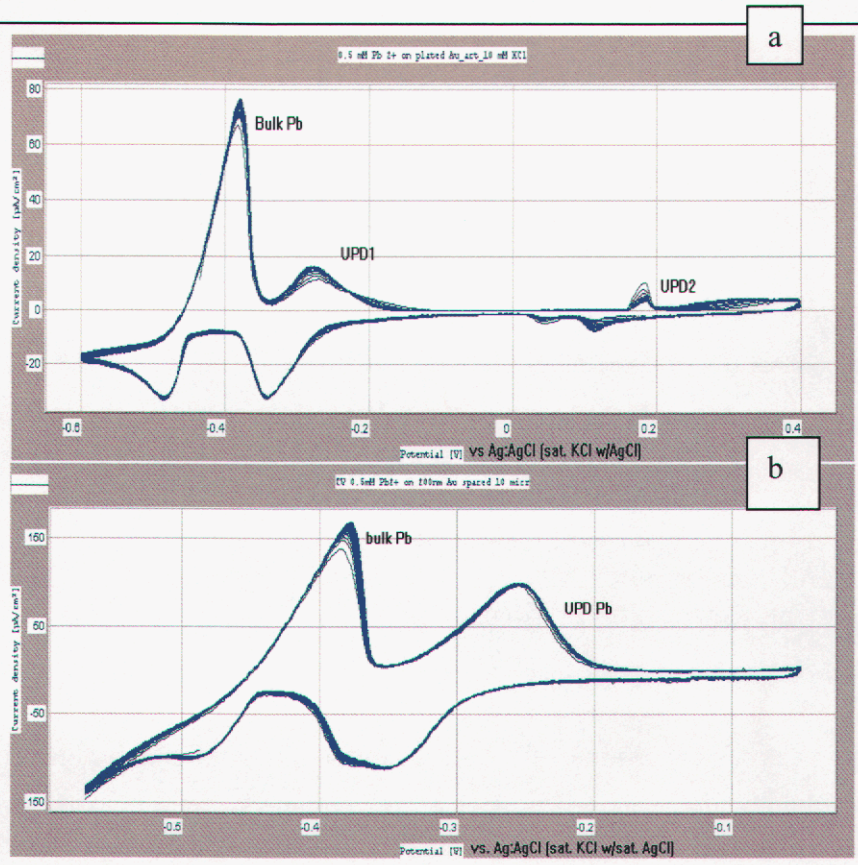

Figure 6.5: Cyclic Voltammetry of 0.5 mM Pb2+ on electroplate gold commercial electrode (a) and gold nano electrode array (below figure a) using 200 nm pores with 10 µm between pores.

- Methods to un-fowling nanoelectrodes required more aggressive electrochemical activation at lower current densities.

6.4 Determination of nanomolar concentrations of lead by Subtractive Anodic-Stripping Voltammetry (SASV) at the Gold Electrode

Subtractive Anodic Stripping Voltammetry (SASV) is similar to Anodic Stripping Voltammetry (ASV) except with the added steps to remove the baseline conditions of the working electrode soon after the ASV is performed. Pictured below are scans from each step in the SASV process (Figure 6.5-Figure 6.10).

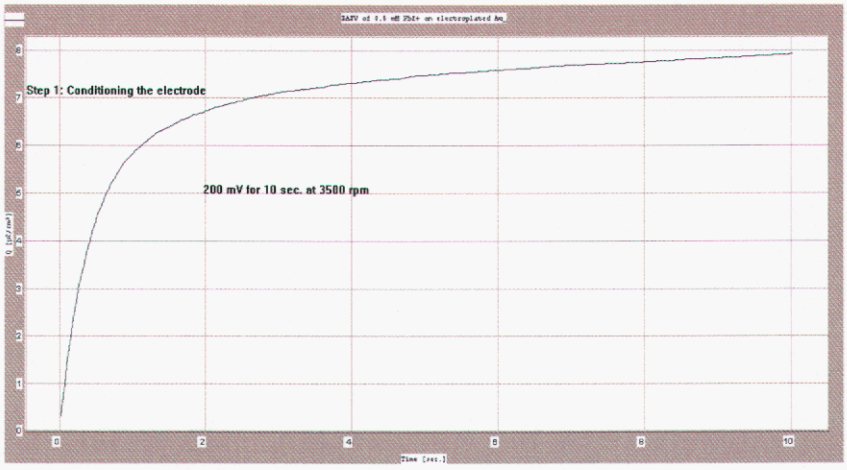

Figure 6.6: Step 1 involves conditioning of the electrode by stripping active ions from the surface using chrono coulometry at an oxidizing potential with strong agitation.

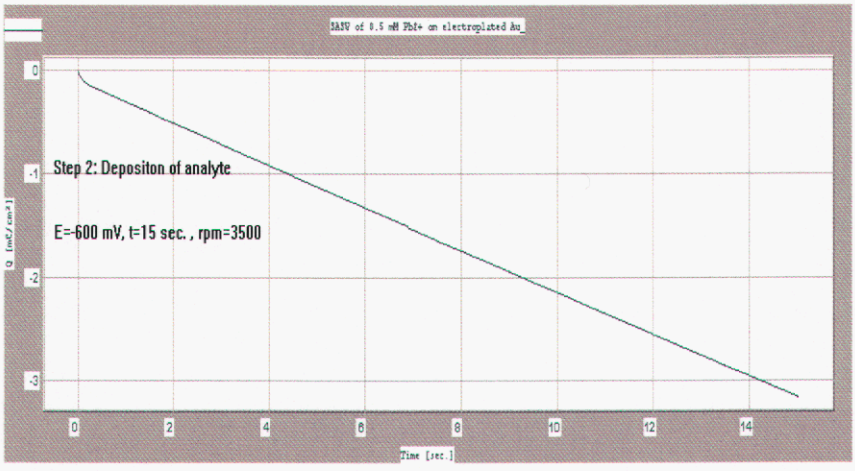

Figure 6.7: Step 2 is the deposition of the active ions on the electrode surface at a fixed reducing potential, this require a chrono coulometry method with strong agitation.

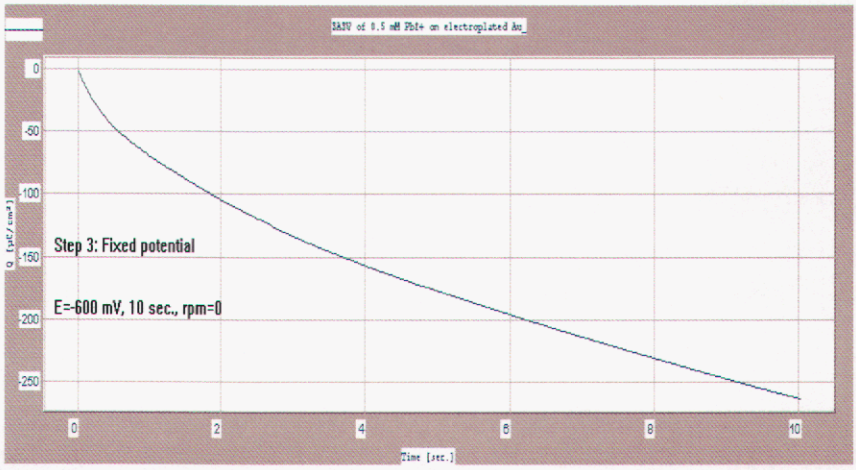

Figure 6.8: Step is a "rest" position with no agitation to strip the diffusion layer of remaining active ions.

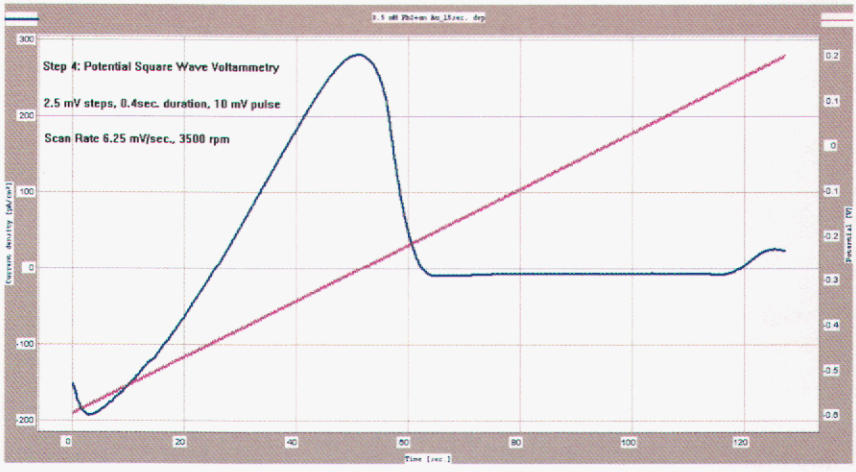

Figure 6.9: Step 4 includes the anodic stripping voltammetry method to measure the peak current as materials are stripped at given potentials.

3.1.1 SASV includes Correction for Background

Key to improving the SASV method:

- UPD plays a central role in the deposition and dissolution steps of ASV.
- Species that exhibit UPD form a monolayer of adatoms, which deposit and strip at potentials more positive than the reversible Nernst potential.
- For nM concentrations, no bulk deposition is invoked for materials that exhibit UPD.
- Technique works best for sub-μM concentrations

Figure 6.10: Step 5 is a repeat of the first four steps without deposition, in other words, in the deposition step, the time is set to zero or not included in the subtractive method. The parameters of this step are more difficult to determine because the diffusion zone around the electro should be free of the ions you are detecting. This should results in a scan of the electrode surface without active ions.

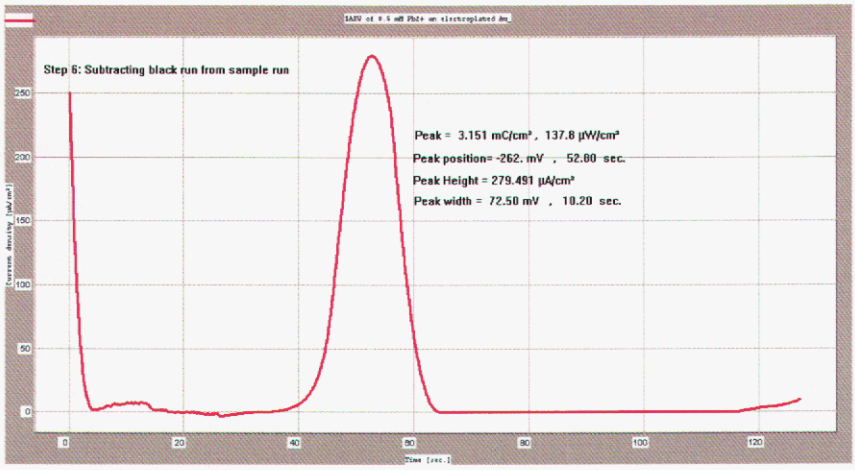

Figure 6.11: Step 6 requires subtracting the results from step 5 from results from step 4. The result gives a well-defined baseline and signal. The signal can easy be analyzed to determine analyte concentration against a standard.

7 Determine detection parameters and characteristics of lead (Pb2+) in water

7.1 Introduction

This section of the project as a whole was undertaken to determine detection properties and characteristics of lead. There were several electrodes used in this project, this section will mainly be concerned with the silver (Ag) working electrode, and the Ag quasi-reference (AgQRE) electrode. Through a series of experiments, we found that Ag is much more effective when testing for limits of detection of Pb^{2+}. Using the commercial Ag working electrode, we were able to detect Pb^{2+} at concentrations as low as 5 nM. However, this was not as easy as it sounds. Throughout these experiments, we found that the conditions of the electrodes and the cell have a considerably large affect on the overall performance of the experiment. Therefore, there are certain precautions that need to be taken into consideration before establishing baseline performance.

We have developed a procedure for cleaning the working electrode and the Ag rod (AgQRE) before they are used. If the electrodes needed to be heavily cleaned and polished, then we stared with a 3-micron polishing paper. The surface of the paper was slightly moistened with DI water, then, the tip of the electrode was polished by softly using figure 8 motions to rub the tip of the electrode on the damp surface of the paper. Once all scratches and residue were removed from the tip of the electrode, we moved on to a different abrasive paper. The next polishing paper used was a 0.5-micron paper. The same exact procedure was used when polishing with this paper. The object of polishing with the 0.5micron paper was to get the electrode tip smooth. The last step to polishing the electrode is to polish using a 0.1-micron paper. The procedure for using the 0.1-micron paper is identical to the others. The purpose for using the 0.1-micron paper is to get the tip as mirror bright as possible. We found that when the electrode needed a quick, non-invasive polishing, the 0.1-micron paper was the only paper that was used. Once the electrode was polished, we placed the tip in a small beaker of DI water. Then placed the beaker and tip in an ultrasonicator for 10 minutes, again in ethyl alcohol for 10 minutes, and finally once more in DI water for 10 minutes. This process was used to remove all residues left over from polishing. That is the steps used for the commercial electrodes. Once the electrode was polished, there was a conditioning process for both the electrodes and the cell.

During the experimentation, we found that the SASV was extremely sensitive to contaminants of any sort. In order to prevent contaminants from interfering with our results, the cell needed to be thoroughly cleaned before usage. We first rinsed the cell with a constant flow of DI water for 5 minutes or greater. Then we used a solution of Alconox cleaner and DI water to scrub the glassware. The cell was then left to soak in the Alconox solution for about 5 minutes. After which it was thoroughly rinsed with regular tap water to break up any left over Alconox that could possibly cause contaminants to enter the experiment. Last, we again rinsed the glassware with DI water. After this the cell remained immaculately clean for experimentation.

Still, the electrodes needed to be conditioned and activated in order to obtain maximum performance when running experiments. In order to do this, a blank solution was composed. The blank solution consisted of 10mM KCl and 10mM HNO_3. The blank solution was poured into the cell and all electrodes were connected to a potentiostat and placed in their respective positions within the experimental set up of the cell. Two sequences were used when activating and conditioning the electrodes. The first was an activation sequence which pulses the electrodes back and forth at a very high potential. The next sequence was a conditioning sequence which runs a standard SASV sequence forty times in succession with each other. Once all these precautionary procedures were completed, both the cell and the electrodes were ready for use in experimental sequences.

7.2 Subtractive Anodic Stripping Voltammetry (SASV)

This experiment was undertaken to determine the limits of detection of Pb^{2+}. The detection limits (**Figure 7.1**) for trace Pb using our standard lab cell was 5nM of Pb in a conductive solution with agitation. A two-electrode system was created using a silver (Ag) working and an Ag quasi-reference electrode was utilized as an Ag rod into which the counter electrode was tied in. Without the conductive salt, we were unable to detect in the range of 5 nM to 35 nM.

7.3 The experiment parameters were as follows:

Step 1: Conditioning

Potential was run at 0mV for 10 seconds at 3500 rpm's. The measuring period was 0.01 seconds.

Step 2: Deposition #1

Potential was run at-700mV for 60seconds at 3500 rpm's. The measuring period was 0.01seconds.

Step 3: Rest # 1

Potential was ran at –700 mV for 7seconds at 0 rpm's. The measuring period was 0.01 seconds.

Step 4: Potential Square Wave #1

The potential range was –700mV through 0mV, pulse 10 mV, amplitude 2.5 mV, scan rate 62.5 mV/sec.

Step 5: Deposition #2

Potential was ran at –50mV for 10 seconds. The measuring period was 0.02 seconds.

Step 5 cont.: Rest #2

Potential was ran at –700mV for 13 sec. The measuring period was 0.02sec.

Step 5 cont.: Potential Square Wave #2

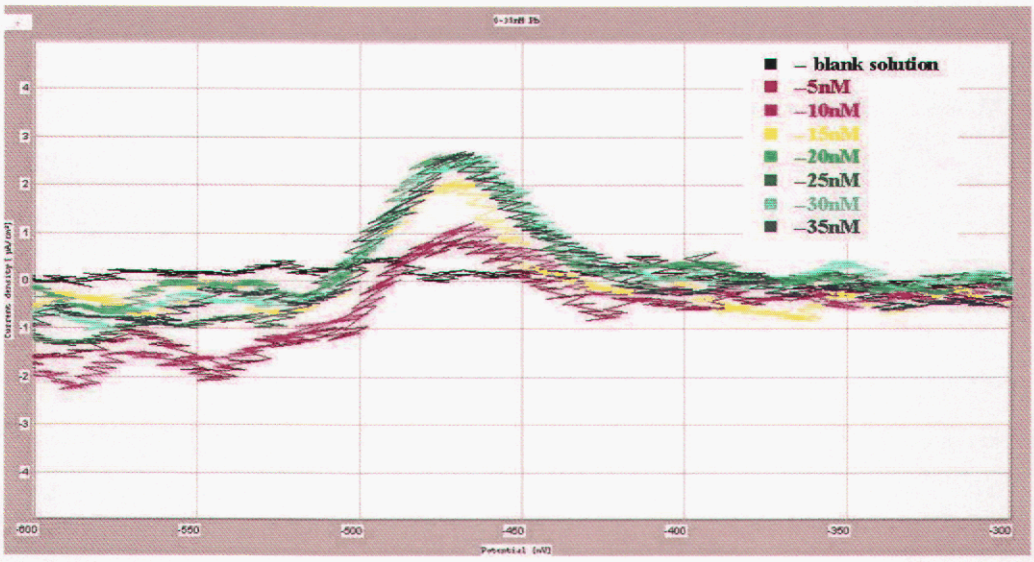

Figure 7.1: Detection of 5 nM-32 nM Pb^{2+} in a solution of 10mM KCL, 10mM HNO_3, working electrode is a 5 mm Ag rotating disk electrode, with an AgQRE counter electrode. The volume of the electrolyte cell was 150ml. Method of analysis was SAVA using 3500 rpm during the stripping

Step 6: Subtract Wave #2 from Wave #1.

Repeat of the sequence used for the Potential Square Wave #1.

There were two open circuits potential sequences placed one at the beginning of the experiment and one at the end of the experiment. Open circuit potential was run for a time period of 6 minutes with a measuring period of 0.2 seconds. The drift threshold was 2 mV/minute. Agitation was used during conditioning 1 and 2, also during deposition 1 and 2.

7.4 Subtractive Anodic Stripping Voltammetry without Agitation

This experiment was undertaken to confirm that the sampling-head and potable Potentiostat system was working correctly, Figure 7.2. The electrodes used were the Ag working electrode, and the Ag quasi-reference electrode. The electrolyte used was composed of 10mM KCl and 10mM HNO_3, and 0.5mM of Pb. The extremely high concentration of Pb was used to ensure that our electrodes would have no problems whatsoever picking up a sizeable Pb peak during the run. The experimental parameters were as follows:

Step 1: Conditioning

Potential was run at 0mV for 10 seconds, 0 rpm's. The measuring period was 0.01 seconds.

Step 2: Deposition #1

Potential was run at-700mV for 60seconds, 0 rpm's. The measuring period was 0.01seconds.

Step 3: Rest # 1

Potential was ran at –700 mV for 7seconds, 0 rpm's . The measuring period was 0.01 seconds.

Step 4: Potential Square Wave #1

The potential range was –700mV through 0mV, 0 rpm's for 0.04sec.

Step 5: Deposition #2

Potential was ran at –50mV for 10 seconds, 0 rpm's . The measuring period was 0.02 seconds.

Step 5 cont.: Rest #2

Potential was ran at –700mV for 13 seconds, 0 rpm's . The measuring period was 0.02sec.

Step 5 cont.: Potential Square Wave #2

The potential range was –700 mV through 0mV, 0 rpm's for 0.04 seconds.

Step 6: Subtracting Wave #2 from Wave #1.

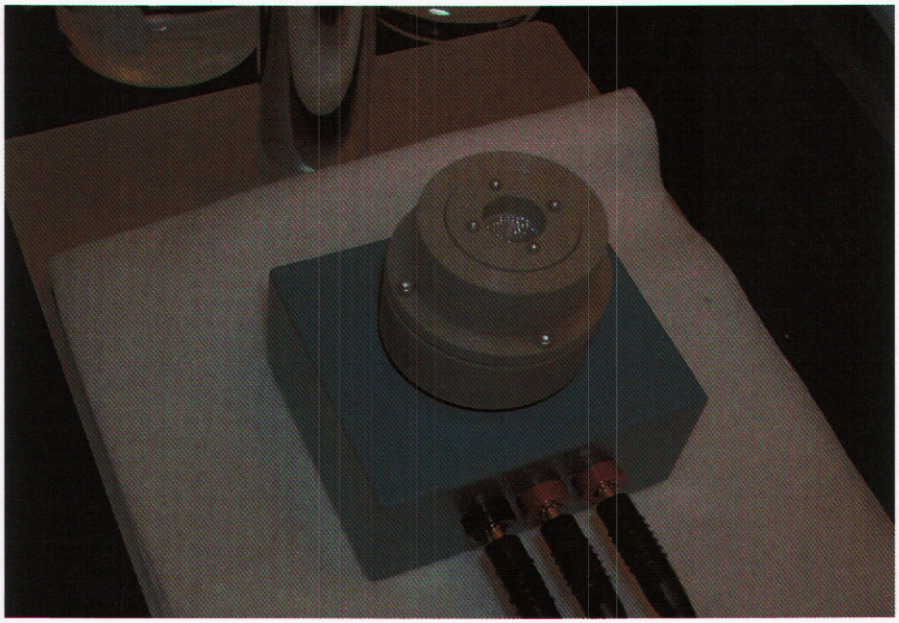

Figure 7.2: Portable sampling head that holds the nanoelectrode arrays, sampling solution and counter electrode. This cell is the field version of the "Lab" cell, which is designed to support the single nano electrode arrays. The counter electrode is a mesh material located above the array.

Again, there were two open circuits potential sequences placed one at the beginning of the experiment and one at the end of the experiment. Open circuit potential was run for a time period of 6 minutes with a measuring period of 0.2 seconds. The drift threshold was 2 mV/minute. Agitation was not used during conditioning 1 and 2, also during deposition 1 and 2. The results (Figure 7.3) of this test produce two peaks, one at the UPD position and a large peak at the bulk deposition position. Since the sample was highly concentrate with lead ions, most of the UPD site were taken followed by deposition of lead on lead at the higher potentials. This result demonstrated the combination of a successful working system including: electrodes, sampling head, and high speed portable potentiostat.

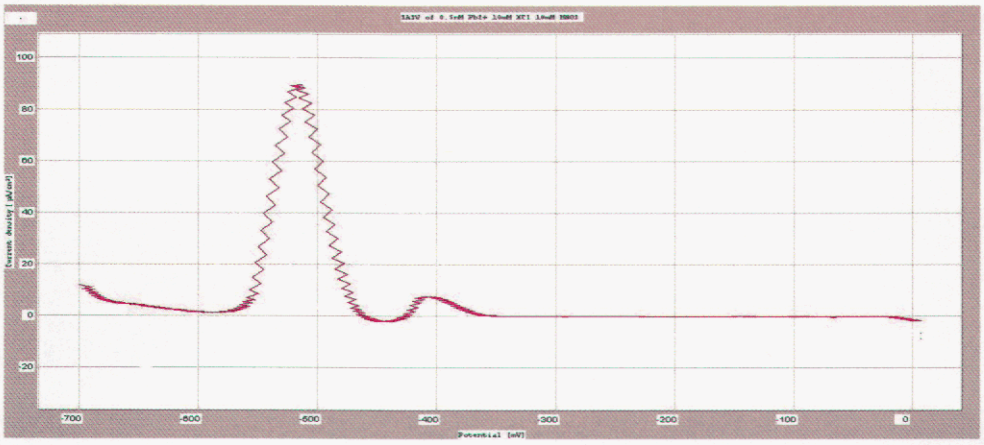

Figure 7.3: SASV scan of 500 μM of Pb^{2+} in 10 mM KCl and 10 mM HNO_3.This scan was produced with out the aid of solution agitation in a two electrode sampling cell. The same cell is designed to hold and contact the nano electrode arrays.

8 Functionalized Electrode Development for Arsenic Detection

8.1 Introduction

A key aspect of the development of electrochemical analysis protocols was the identification and evaluation of appropriate working electrodes for selective analysis of target analytes. Per the recommendations of experts in Sandia's Water Initiative, we focused our attention on the quantitative speciation of arsenic in water samples. Here, the objective was the quantitative determination of As(III), As(V), and total As in groundwater samples and/or municipal water supplies. The constraint on our electroanalytical procedure that differentiated it from other published reports on arsenic determination is that it was to be performed without addition of supporting electrolyte or reducing agent to the water sample. We developed a three-phase approach for our protocol development activity: (1) using conventional (*e.g.*, 3 mm diameter) voltammetric working electrodes, demonstrate in the lab the ability to quantitatively determine As(III) and As(V) in water using supporting electrolyte but no homogenous reducing agent to convert electroinactive As(V) to electroactive As(III); (2) using nanoelectrode arrays, perform lab measurements of As(III) and As(V) in untreated aquifer water; and (3) in the field, use nanoelectrode arrays and the high-speed potentiostat to quantitatively determine As(III) and As(V) in untreated environmental and municipal water samples. We focused our attention on the first phase of this approach during FY02 and FY03 and those results are described in this section of the report. Due to budget reductions and task reprioritizations, the second and third phases were not included in the project plan for the final year of the project (FY04).

As(III) is readily and directly determined by voltammetry, based on numerous reports in the literature. For example, anodic stripping voltammetry has been used to measure As(III) at sub-parts per billion (ppb) concentrations at a gold working electrode. In contrast, As(V) is considered electroinactive by most researchers and is typically converted to As(III) for analysis using reducing agents such as sulfur dioxide, sodium sulfite, L-cysteine, hydrazine dihydrochloride, mannitol, or pyrogallol. Only a few published reports [for example, reference 1] describe direct voltammetric determination of As(V), *e.g.*, by anodic stripping voltammetry following deposition at extreme cathodic potentials (-1.6 volts vs. Ag/AgCl). Our laboratory experiments revealed this to be a very difficult analysis since copious hydrogen evolution at the working electrode negatively affected accuracy and precision and also introduced practical problems related to adherence of gas bubbles to the electrode surface. To circumvent these problems, we explored the use of chemically modified electrodes for direct As(V) measurement. Our strategy was to incorporate the reducing agent into the working electrode to electrocatalytically assist the reduction of As(V) to As(0) so that it occurs closer to its standard electrode potential and without concomitant production of hydrogen gas. We synthesized poly(pyrogallol)-modified electrodes by anodic polymerization of pyrogallol from aqueous solutions onto glassy carbon working electrodes (Figure 8.1). These electrodes show good electrochemical activity for the ferricyanide/ferrocyanide redox couple commonly used as a test analyte for electrochemical analysis (Figure 8.2). They were also demonstrated to be functioning working electrodes for electrochemical analysis

of As(III) and As(V) (Figure 8.3 and Figure 8.4). Here, we used the poly(pyrogallol) modified electrodes in a three-step electrochemical protocol: (1) preconcentration of As(III) and As(V) within the pyrogallol polymer at open circuit from water samples at neutral pH; (2) electrocatalytically-assisted reduction of As(III) and As(V) to As(0) in 1 M HCl; and (3) anodic stripping voltammetry in 1 M HCl for determination of arsenic concentration. Combining the results of this poly(pyrogallol)-based analysis with published procedures for As(III) determinations provides the desired speciation of As(III) and As(V). As seen in Figure 8.4, our procedure for the direct determination of As(V) at poly(pyrogallol)-modified electrodes was demonstrated at parts-per-million (ppm) concentrations, well above the target detection limits of 5 parts-per-billion (ppb). However, the dramatic improvements (~1000X) in sensitivity expected with the implementation of nanoelectrode arrays could extend the usefulness of this chemically modified electrode approach to the desired detection limits.

8.2 References

1. U.S. Environmental Protection Agency Method 7063, "Arsenic in Aqueous Samples and Extracts by Anodic Stripping Voltammetry", December 1996.

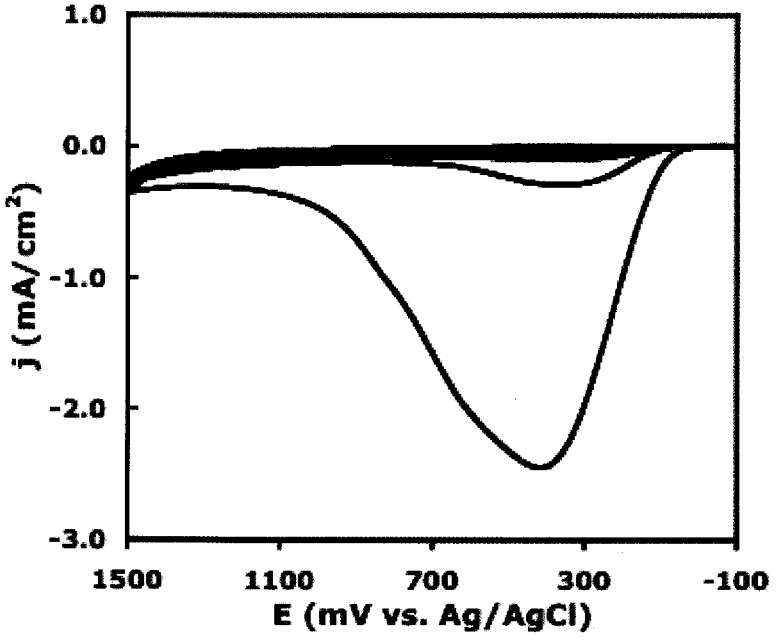

Figure 8.1: Anodic polymerization of pyrogallol onto glassy carbon working electrode. Supporting electrolyte: 0.1 M potassium phosphate buffer, pH 7. Pyrogallol concentration: 11 mM. Scan rate: 20 mV/s. Cyclic voltammetry: 10 scans between –100 and +1500 mV vs. Ag/AgCl reference electrode.

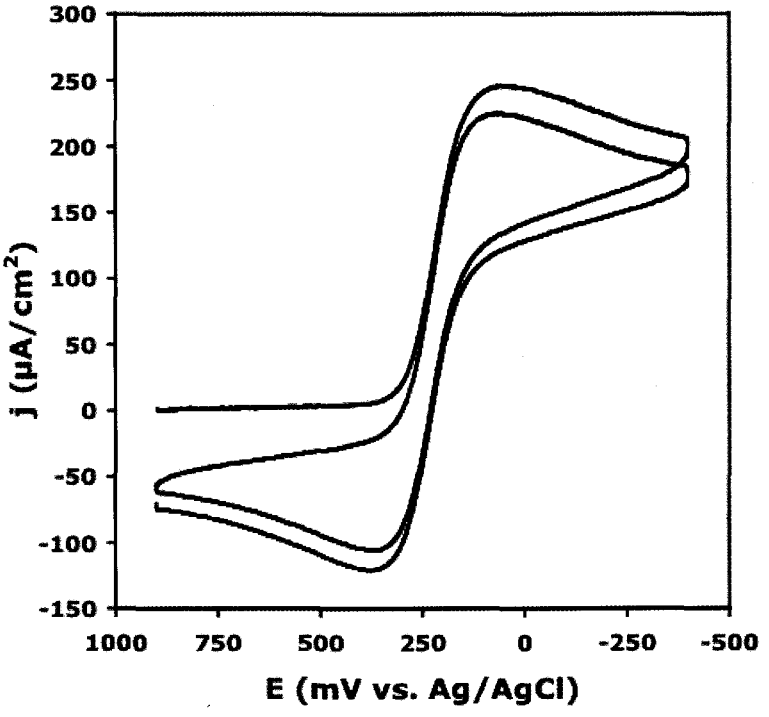

Figure 8.2. Cyclic voltammetry of 5 mM $K_3Fe(CN)_6$ at the poly(pyrogallol) modified glassy carbon electrode prepared in **Figure 8.1**. Supporting electrolyte: 0.1 M potassium phosphate buffer, pH 7. Scan rate: 100 mV/s. Cyclic voltammetry: 2 scans between +900 and –400 mV vs. Ag/AgCl reference electrode.

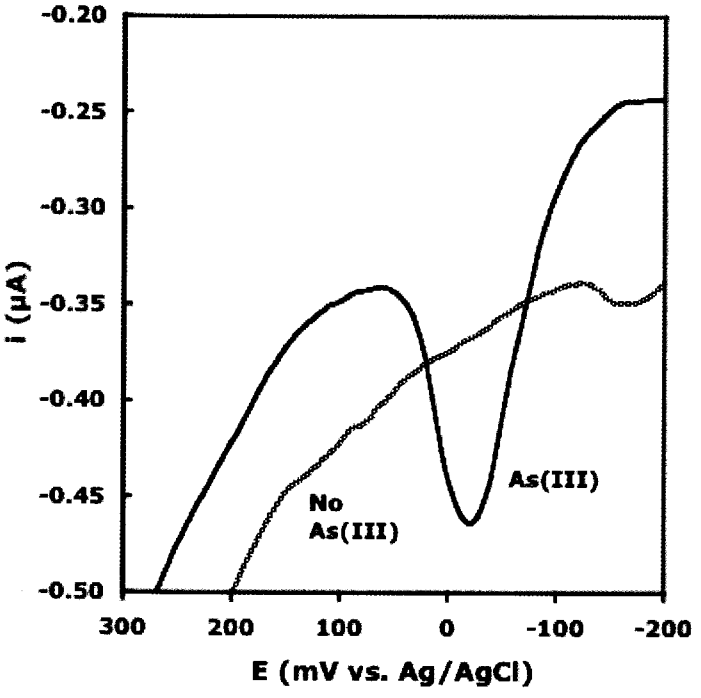

Figure 8.3. Differential pulse anodic stripping voltammetry of As(III) at a poly(pyrogallol) modified glassy carbon working electrode following open circuit accumulation of As(III) onto working electrode in 0.1 M potassium phosphate buffer, pH 7. Supporting electrolyte for DPASV: 1 M HCl. As(III) concentration: 1.7 ppm. Scan rate: 10 mV/s.

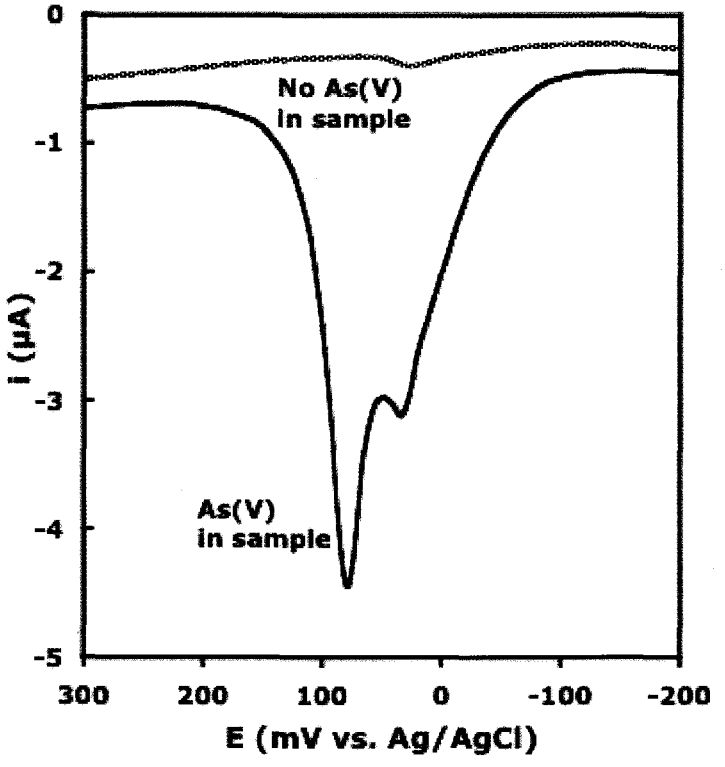

Figure 8.4. Differential pulse anodic stripping voltammetry of As(V) at a poly(pyrogallol) modified glassy carbon working electrode following open circuit accumulation of As(V) onto working electrode in 0.1 M potassium phosphate buffer, pH 7. Supporting electrolyte for DPASV: 1 M HCl. As(V) concentration: 1.7 ppm. Scan rate: 10 mV/s.

9 High-Speed Transient Potentiostat for High-Density Nanoelectrode Arrays

9.1 Introduction

Analysis of transient electrochemical signals requires the ability to source rapid, precise waveforms across the electrochemical cell (nano-electrode array). These waveforms are generally multi-level and can be as narrow as 4 µsec in peri Microcontroller in H_2O,

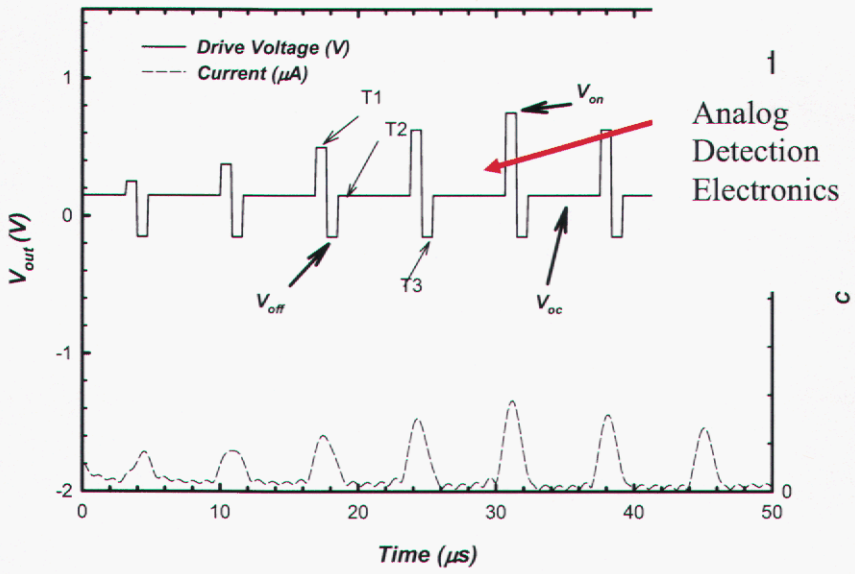

Figure 9.1: Figure showing generalized waveform that can be produced from the poteniostat.

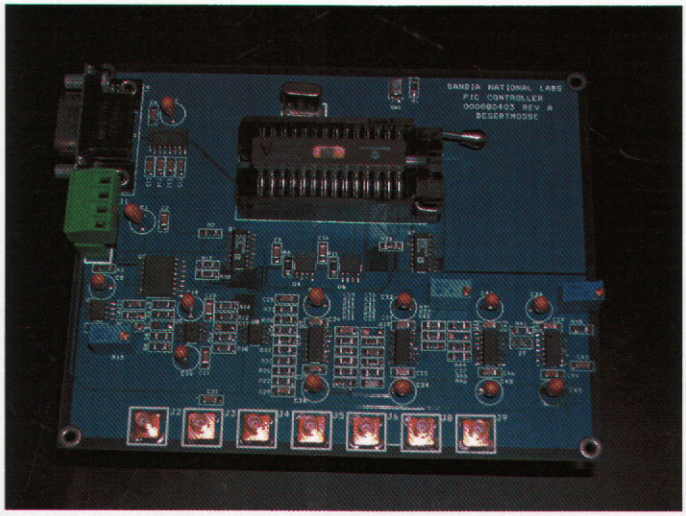

Figure 9.2: Photograph of the *High-Speed Transient Potentiostat* illustrating the analog circuitry and the microcontroller.

potential differences across the cell are generally less than 0.83 V to preclude the

production of $H_2(g)$ which will form bubbles on the surface and inhibit the diffusion of ions back to the cell. We have developed a *High-Speed Transient Potentiostat* that can produce multiple pulses with varying potential levels between –1.2 V and 1.2 V and can return to a voltage equal to the open circuit voltage of the cell within intervals of less than 4 μsec. The circuit can produce the generalized waveform illustrated in Figure 9.1. In Figure 9.1, the trace labeled *Drive Voltage* is the potential that is placed across the nanoelectrode array, where V_{on} (referenced to V_{OC}) is provided as the cell stimulus for a selected period of time (*T1*) followed by V_{off} (referenced to V_{OC}), for time *T2* followed by the a quiescent period (*T3*) during which the circuit is provided a voltage equivalent to the *open circuit* voltage (V_{OC}) of the cell. This is done so that no current will flow into the electrometer that is driven by the cell potential. The trace in Figure 9.1 labeled *Current* is a representation of the expected current into the electrometer section of the circuitry.

9.2 System Design

A photograph of the system is provided in Figure 9.2, and block diagram of the system is illustrated in Figure 9.3 showing the basic functions of the system. The system is based on a PIC16C62B[1] micro-controller that communicates with the internal components of the system controlling the amplitude and timing of the stimulus pulses, monitors the value of the open circuit voltage (V_{OC}) and supplies it back to the cell, communicates via RS-232 to a main control computer (laptop or palmtop), and returns the measured information to the main control computer. The system can be programmed to return the integrated current from high-speed transient pulses, the instantaneous current during a cyclic voltammetry or stripping voltammetry measurement, or return the open circuit

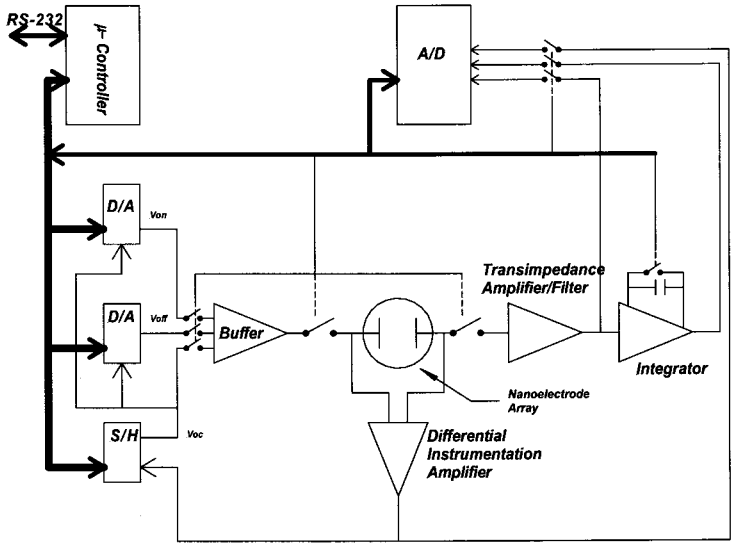

Figure 9.3: Block diagram of the potentiostat illustrating the μ-controller, analog to digital (A/D) converter, digital to analog converters (D/A), buffer amplifier, differential amplifier, trans-impedance amplifier, integrator, and nano-electrode array.

voltage measured. The system utilizes a series of ADG431[2] precision quad single-pull-single-throw (SPST) switches wired to rapidly provide various voltages to the cell and to

isolate the cell from the rest of the circuit to allow accurate measurement of V_{OC}. The normally open switches are wired in a bipolar mode where current can flow in either direction through the switch, and are controlled using a standard TTL level where the input is active low.

As shown in Figure 9.3 (for circuit details see Appendix B), the switches from the digital-to-analog (D/A) converters (MAX5541[3]) and the sample-and-hold (S/H) amplifier (LF398A[4]) are connected via ADG431 switches to a buffer amplifier (LF353[4]) that is in turn connected to the cell. The D/A's are programmed serially via a three-wire interface that includes a chip select (CS), data line (DOUT), and serial clock line (SCLK). Since the devices are programmed serially, it is impractical to generate the waveform directly from the D/A circuits due to speed considerations. Thus, two D/A circuits are employed along with the S/H amplifier and switches to generate the waveform. This approach is illustrated in Figure 9.3 where each of the switches driving the buffer are alternately closed allowing that signal to be placed on the cell. Since the output values are

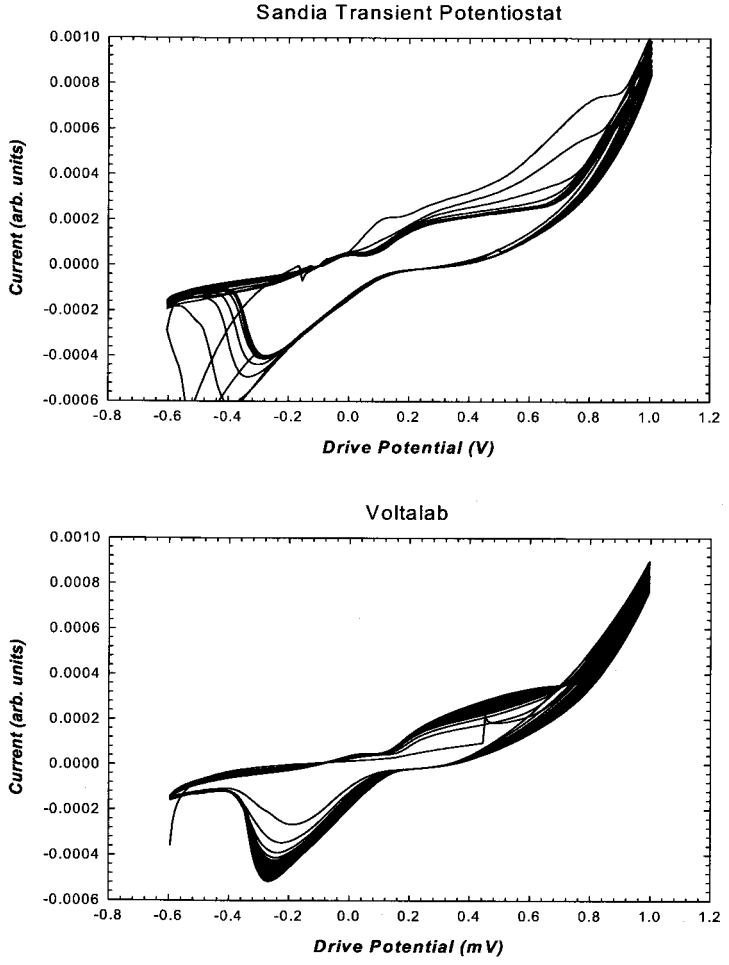

Figure 9.4: Plot of response of electrochemical cell measured on Sandia transient potentiostat compared to commercial *Voltalab* instrument during cyclic voltammetry experiment. Electrochemical cell was produced by placing two Cu electrodes in a solution of 0.118 gm of NaCl dissolved in 200 mL of deionized H_2O with approximately 0.1 mL of KNO_3 solution. Both instruments show the same basic behavior with appropriate peaks occurring at the same potential as the input potential is varied.

preprogrammed into the D/A converters, the micro-controller only must switch the signals onto the buffer which can be accomplished with 200 nsec resolution allowing adequate speed. This is a factor of 32 times faster than what would be possible using this 20 MHz controller to generate the signals from the D/A converters directly. In addition, this architecture allows for direct measurement of the open circuit voltage across the cell and its direct reintroduction to the cell via the sample-and-hold circuit that constitutes an analog memory.

Measurement of the open circuit voltage is accomplished by opening both switches adjacent to the cell to isolate it from the rest of the circuit (S3A and S2D Appendix B). The switches have open circuit impedance on the order of $1x10^{11}\ \Omega$ which provides adequate isolation from the rest of the drive circuitry. The voltage across the cell is then measured using a differential instrumentation amplifier constructed from LF347[4] operational amplifiers that also provide $10^{12}\ \Omega$ input impedance. This isolates the cell from any current leakage path that would disrupt the measurement of V_{OC}. The output of the instrumentation amplifier is input into the S/H amplifier, which is actuated by the micro-controller and produces an analog voltage equal to V_{OC}. This is then available for re-injection into the cell drive circuit. In addition, the output of the sample-and-hold amplifier can be read digitally via the A/D converter (MAX187[3]). The value of V_{OC} is reintroduced to the drive potential via an adding opamp circuit with the outputs from each of the D/A converters (U5B Appendix B).

To measure the cell current, the switches adjacent to the cell are closed and the current is converted into a voltage using a trans-impedance amplifier followed by a low-pass filter. The circuit is constructed from LF347 operational amplifiers and has a trans-impedance gain of $10^4\ \Omega$. The low-pass bandwidth of the filter is on the order of 10^6 Hz to accommodate the rapid pulses possible from the pulse generation section of the circuit. That signal is then input into an integration circuit (U10A Appendix B) allowing the sum of the current from several pulses to be stored and then read using a 12-bit resolution A/D converter circuit (MAX187[3]). Using an integration circuit allows adequate bandwidth to be designed into the trans-impedance amplifiers to accommodate the rapid pulses while eliminating the Nyquist sampling issues that normally must be addressed in high-speed systems. The tradeoff is a loss of signal shape which can be obtained, if required, by connecting a fast oscilloscope to the supplied SMB connector (J5) at the output of the trans-impedance amplifier (see Figure. 12.1 and Figure 12.2). A final ADG431 switch is used in parallel to the integration capacitor to allow reset of the integrator as illustrated in Figure 9.3.

The *High-Speed Potentiostat* control system is capable of operating in a traditional potentiostat mode allowing cyclic voltammetry and subtractive anodic stripping voltammetry (*SASV*). Since these operational modes are slow compared to the transient signals that the system was originally designed to produce and measure, we have incorporated jumpers (J10, J7, and J8) to bypass the low frequency poles of the filter allowing operation in the DC-10^6 Hz frequency bands. However, this introduces DC voltage errors from operational amplifier leakage current in the circuit.

9.3 System Verification

Figure 9.4 shows the response of the transient potentiostat compared to the response from a commercial instrument to a baseline electrochemical cell in cyclic voltammetry mode. These data indicate that after several cycles, the response of both instruments converges to an equivalent shape as a function of voltage. These data illustrate that the instrument's performance is similar to a commercial instrument in the slow cyclic voltammetry mode indicating that the signal producing sections of the circuit and the measurement sections of the circuit are working reproducibly and predictably. The data in Figure 9.4 were read using an external HP3478A voltmeter. However, in the newest version of the instrument, the instantaneous current at J9 can be read directly via the on-board A/D converter and sent to the PC controller allowing a more compact and portable instrument.

Typical data obtained from the on-board A/D via RS-232 is shown in Figure 6.4 for a Pb electrochemical cell with 0.5 mM Pb^{2+} dissolved in 10 mM KCl and H_2O. The system is operated in SASV mode and again shows very good agreement with the commercial Voltalab[5] instrument.

9.4 High-Speed Data Acquisition

The A/D converter communicates with the micro-controller using a similar three-wire interface as the D/A converters. In the high-speed mode, the system architecture is designed so that a simple algorithm for computing an average current is available via the micro-controller hardware. Although the 8-bit micro-controller has limited floating point computing capability and limited memory, it is possible to compute an average of the cell

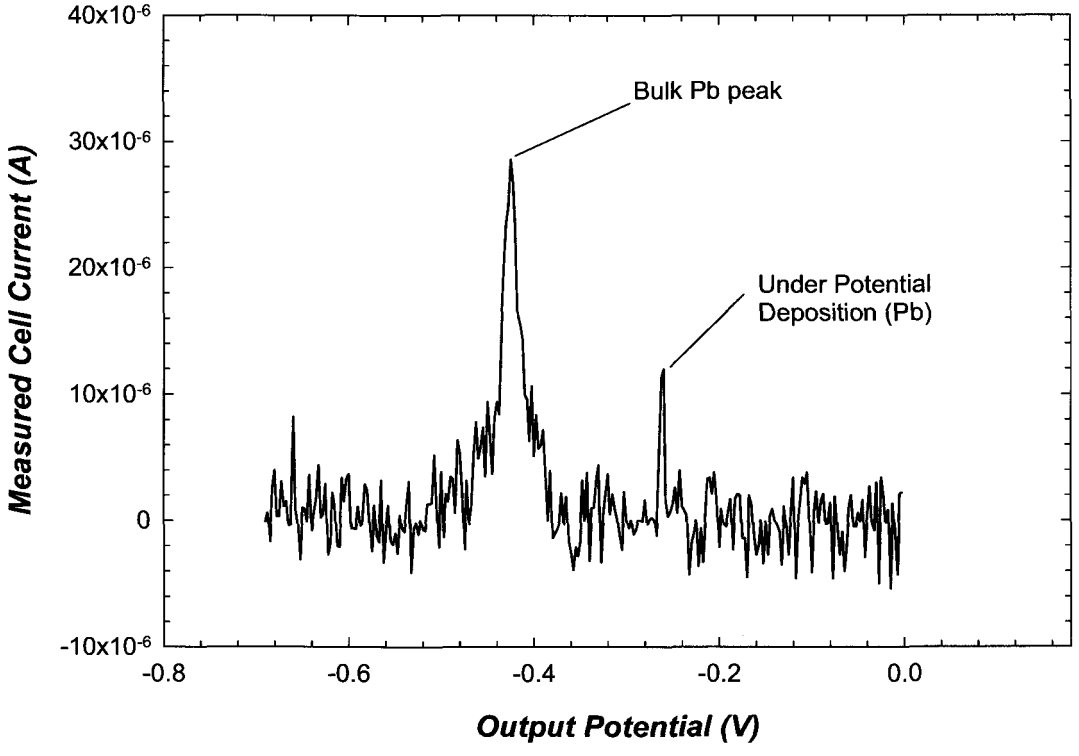

Figure 9.5: Data showing Pb peak in electrochemical cell measured using the *High-Speed Transient Potentiostat* in subtractive anodic stripping voltammetry (SASV) mode.

current for a fixed set of voltage levels (V_{on} and V_{off}) provided that 2^n samples are acquired by the integrator. If the micro-controller is programmed to send 2^n pulses to the cell, the total integrated voltage output from the integrator will be the sum of the current pulses from the cell. This value is then arithmetically shifted to the right by n places, the result is the average signal measured by the trans-impedance amplifier. Written mathematically for 2^n samples:

$$\overline{V} = \frac{\sum_{i=1}^{n} V_n}{n} \tag{9.1}$$

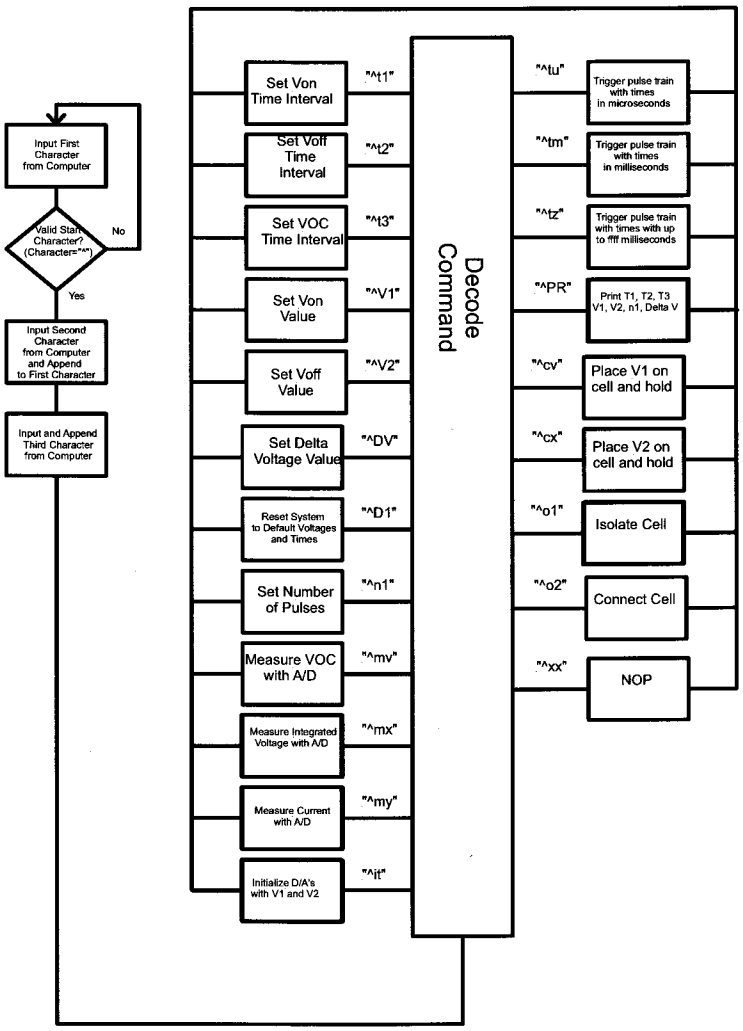

Figure 9.6: Micro-controller program flow chart illustrating the various commands and resulting actions from the micro-controller.

where $\overline{V}$ is the average output voltage and $\sum_{i=1}^{n} V_n$ is the value at the output of the integrator as measured by the A/D converter. This function is both easily and efficiently accomplished in the micro-controller program for the special case of 2^n samples because of the availability of the arithmetic shift left function as a native assembler command for the micro-controller. Any number of samples other than 2^n samples will require floating point mathematics which consumes both operational speed and limited program memory.

9.5 System Control

The program functions that have been written to control the circuit are provided in Appendix A and correspond to the schematic provided in Appendix B. The program is written in the C-language and is compiled into the reduced instruction set assembly programming set native to the micro-controller using *PIC micro® MCU C* Complier.[6] The program is designed to operate in a slave mode from the main control computer using a simple RS-232 interface. The generalized flow of the program is provided in Figure 9.6 illustrating the major architecture of the program. The majority of the time the program is in a loop that inputs characters from the RS-232 interface. All valid commands to the system are prefixed by the character "^" (ASCII code hex 5E) which must be sent in order for the program to proceed to the next step. If a valid "^" is detected, then the next two ASCII characters are appended to the "^" and the resulting three character code is passed into a decoding structure. This is written as a "SWITCH-CASE" structure in the C-language and allows for multiple system actions based on the input command as shown. For a detailed description of the function of each code, see the program printout in *Appendix A*. A listing of the system commands and function are given below in Table 9.1.

Table 9.1: Table of System Commands

Command Sequence	Function	Data Format
^t1	Set period of time in μsec for V_{on} to remain at cell input. Data is in hexadecimal (01_{16}-FF_{16})..	^t1[MSB][LSB]<cr>
^t2	Set period of time in μsec for V_{off} to remain at cell input. Data is in hexadecimal (01_{16}-FF_{16})..	^t2[MSB][LSB]<cr>
^t3	Set period of time in μsec for V_{OC} to remain at cell input. Data is in hexadecimal (01_{16}-FF_{16})..	^t3[MSB][LSB]<cr>
^V1	Set amplitude in volts for V_{on} at cell input. Data is in hexadecimal (01_{16}-FF_{16})..	^V1[MSB][LSB]<cr>

^V2	Set amplitude in volts for V_{off} at cell input. Data is in hexadecimal (01_{16}-FF_{16})..	^V2[MSB][LSB]<cr>
^DV	Set amplitude in volts for *delta V* at cell input. Data is in hexadecimal (01_{16}-FF_{16})..	^DV[MSB][LSB]<cr>
^VC	Update value on S/H..	^VC<cr>
^D1	Reset system to default condition. (*T1=T2=10μsec,* $V_{on}=V_{off}=0$)	^D1<cr>
^n1	Set number of pulse sequences to send to cell. Data is in hexadecimal (01_{16}-FF_{16}).	^n1[LSB]<cr>
^mv	Initiates a read of the open circuit voltage from the A/D converter and returns voltage in two 8-bit bytes followed by a <cr><lf>.	^mv<cr> Return: [V_{msb}][V_{lsb}]
^mx	Initiates a read of the integrated current in terms of voltage from the A/D converter and returns voltage in two 8-bit bytes followed by a <cr><lf>.	^mx<cr>
^my	Initiates a read of the instantaneous current in terms of voltage from the A/D converter and returns voltage in two 8-bit bytes followed by a <cr><lf>.	^my<cr>
^it	Initiates the voltage programmed into V1 and V2 to the respective D/A converters.	^it<cr>
^tu	Initiates a pulse train as programmed from V1, V2, t1, t2, t3, and n1 with time measured in microseconds. (delays up to $00ff_{16}$	^tu<cr>

	microseconds)	
^tm	Initiates a pulse train as programmed from V1, V2, t1, t2, t3, and n1 with time measured in milliseconds. (delays up to $00ff_{16}$ milliseconds)	^tm<cr>
^tz	Initiates a pulse train as programmed from V1, V2, t1, t2, t3, and n1 with time measured in microseconds and long integers. (times up to $ffff_{16}$ microseconds)	^tz<cr>
^PR	Returns values of T1, T2, T3, V1, V2, n1, DV in four bytes followed by a <sp>.	^PR<cr> Return: $T1_{msb}T1_{lsb}$<sp> $T2_{msb}T2_{lsb}$<sp> $T3_{msb}T3_{lsb}$<sp> $V1_{msb}V1_{lsb}$<sp> $V2_{msb}V2_{lsb}$<sp> $n1_{msb}n1_{lsb}$<sp> $DV_{msb}DV_{lsb}$
^cv	Place voltage V1 on cell and hold.	^cv<cr>
^cx	Place voltage V2 on cell and hold.	^cx<cr>
^o1	Isolate cell from drive potential.	^o1<cr>
^o2	Expose cell to drive potential.	^o2<cr>
^XX	Performs no operation. Returns to beginning of program. XX represent any sequence not listed above.	^XX<cr>

9.6 Calibration

In order to translate the hex data input into the system and received from the system to actual voltage, it was necessary to perform calibrations of the D/A converters and the A/D converter. This was done by measuring the output of the D/A converters using an HP3457A voltmeter and comparing that voltage to the hex value sent to the D/A converters. Similarly, the A/D converter was calibrated by measuring the input to the A/D with an HP3457A voltmeter and then comparing that reading to the output of the

D/A converter. By inserting a cell of known stable resistance (a series resistor of 17.8kΩ) into the system and measuring the output, it is possible to ascertain a calibration in terms of cell current. The results from these measurements are shown below in Figure 9.7 and Figure 9.8. In Figure 9.7, the output of the D/A converters is plotted as a function of the input value represented in base 10. For the A/D 1 we have the following calibration curve:

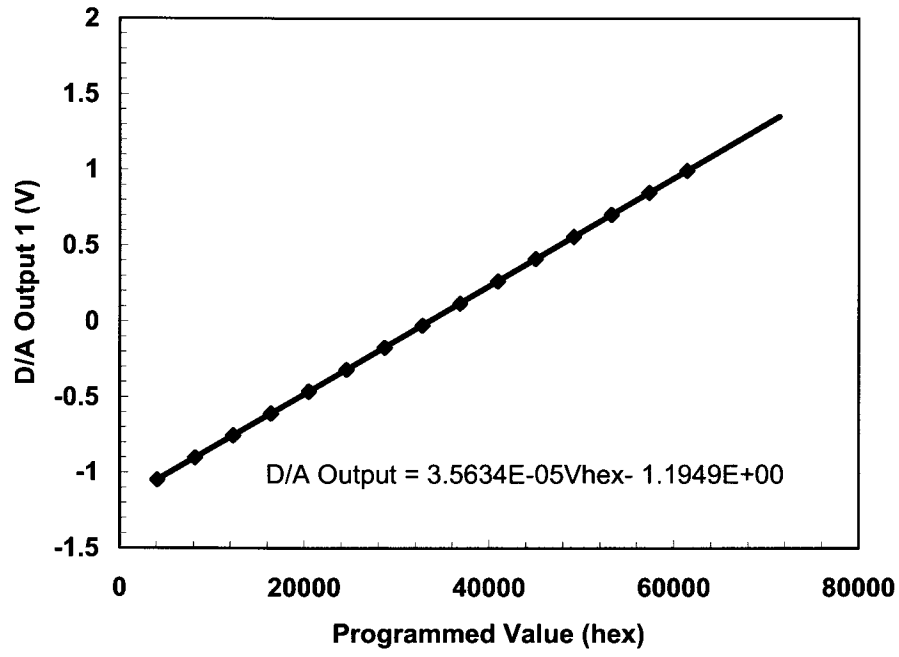

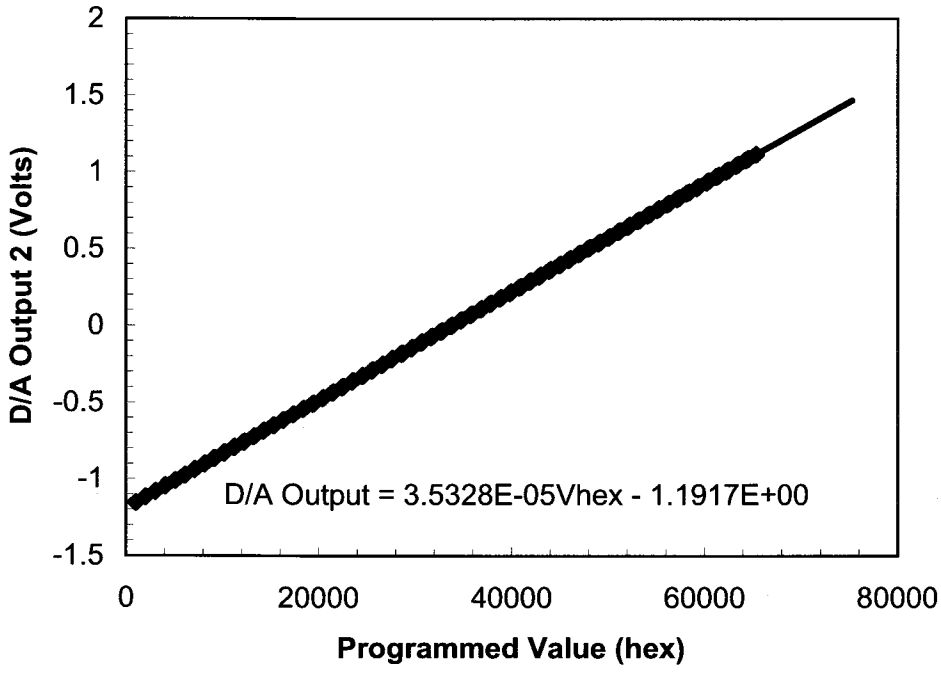

Figure 9.7: Calibration plots of D/A outputs as a function of input value for D/A 1 and D/A 2. Input is in hex but scale is represented in base 10. Calibration equation is given on each page.

$$V_{hex} = \frac{V + 1.195}{3.56 \times 10^{-5}} \tag{9.2}$$

For the A/D 1 we have the following calibration curve:

$$V_{hex} = \frac{V + 1.19}{3.533 \times 10^{-5}} \tag{9.3}$$

In the above equations, V is the desired output in volts and V_{hex} is the value (base 10) that

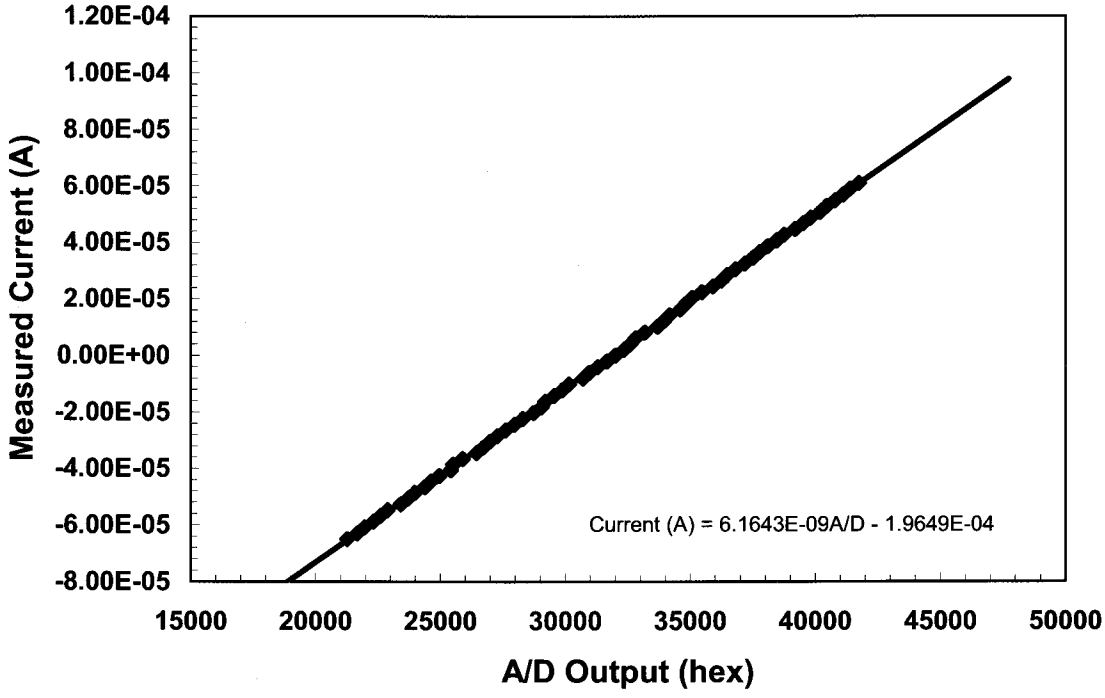

Figure 9.8: Plot of current as a function of A/D output. Output response was measured using an HP3457A multimeter with a fixed cell of 17.8kΩ. Ohm's law provides the actual current and the result is compared to the A/D output in the plot.

when converted to hex and sent to the D/A converter will produce the desired voltage for each channel.

For data read from the circuit, the hex value converted to current is the following:

$$I = 6.16 \times 10^{-9} V_{A/D} + 1.965 \times 10^{-4} (Amps) \tag{9.4}$$

Where $V_{A/D}$ is the output number sent from the A/D converter and I is the corrected current in amps. Thus, the measured current in Amps is found by substituting the hex value returned from the A/D into equation 4.

9.7 System Control Software

The control program to operate the system was written in *Agilent Vee*[7] and simply performs the function of sending data to the instrument and receiving it, processing it through Eqs. (9.2), (9.3), and (9.4) to convert to voltages from hex values and providing the interface with the operator. Potential profiles are specified at this level in the system and this allows for a simple to read and operate user interface with the operator. Since

this system interfaces with the computer via a common RS-232 type interface, operation can be accomplished via any common laptop or palm type controller via a run-time version of the control software. All of the higher level calculations that must be done in floating point are completed in the "Vee" program since the controller has a more sophisticated processor. Figure 9.9 is a screen shot of the program interface with the top left hand plot being the cell potential profile as a function of time, the top right hand plot being a plot of the corresponding cell current as a function of time, and the bottom plot being the difference between the two currents for the two potential ramps with the horizontal axis being potential and the vertical axis being current. The user interface can be made more sophisticated to allow for more analysis algorithms, drop down menus of potential contaminates, controls for variation of parameters, and any other function a user could require.

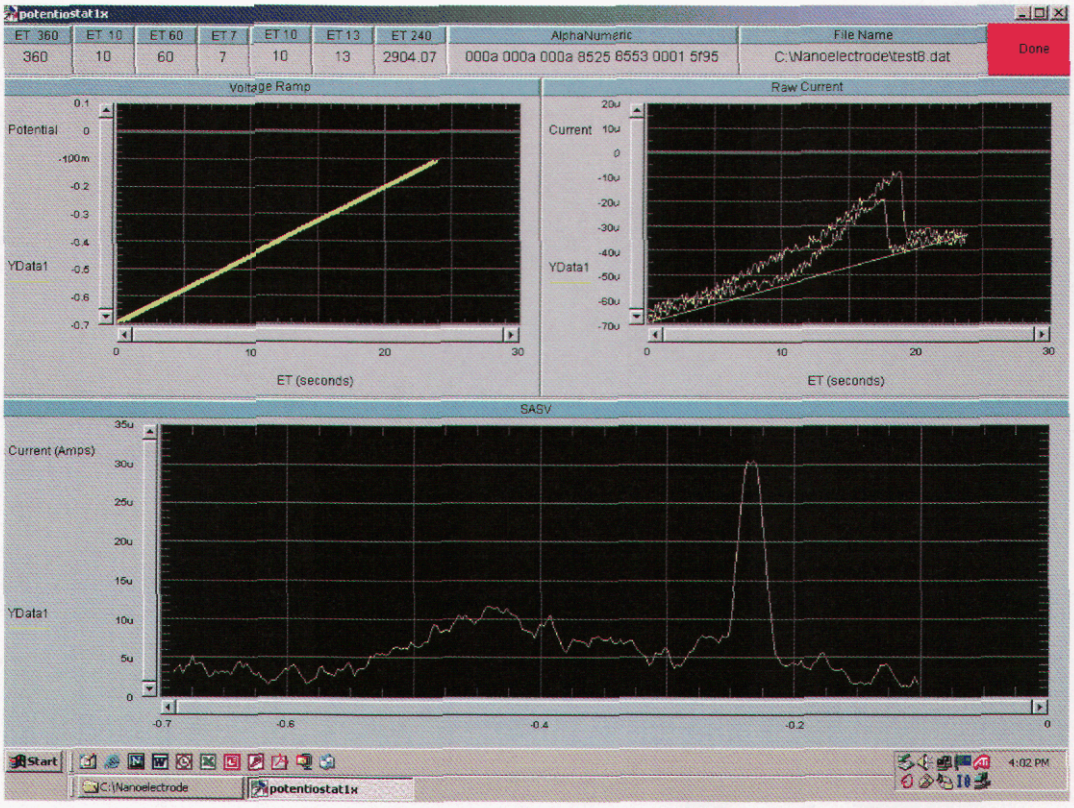

Figure 9.9: Screen shot of the Agilent Vee software interface for an experiment with Pb in H_2O. System reports the potential profile and the current as function of time during the scan (top two graphs) and the difference between the two current graphs (lower graph) or the SASV result. All higher order floating point calculations and conversions from hex to real numbers is accomplished in the "Vee" program with the laptop's more sophisticated processor.

9.8 Conclusion

We have developed a *High-Speed Transient Potentiostat* that can measure the current from nano-electrode arrays with a time resolution on the order of microseconds. The device has 21 control functions and can be demonstrated in the "slow" mode for cyclic

voltammetry and subtractive anodic stripping voltammetry or the "fast" mode for transient measurements. We have demonstrated the system in the cyclic voltammetry and subtractive anodic stripping voltammetry modes and found favorable comparison to commercial hardware. Calibrations have been performed to allow conversion between internal hex values and real voltages from the system. We have described the system architecture and the "firmware" in the system controller along with the control functions. Results from actual nano-electrode arrays are still pending but functional tests of the instrument are complete and results are promising.

9.9 References

[1] Microchip Technology Inc., 2355 W. Chandler Blvd., Chandler AZ 85224, USA.

[2] Analog Devices, One Technology Way, P.O. Box 9106, Norwood, MA 02062-9106, USA.

[3] Maxim Integrated Products, 120 Sand Gabriel Drive, Sunnyvale, CA 94086, USA.

[4] National Semiconductor Corporation, 2900 Semiconductor Drive, P.O. Box 58090, Santa Clara, California, USA 95052-8090

[5] Radiometer Analytical SAS, 72 rue d'Alsace, 69627 Villeurbanne CEDEX, Lyon, France.

[6] Custom Computer Services, Inc. P.O. Box 2452, Brookfield, WI 53008, USA.

[7] Agilent Technologies, Inc. Headquarters, 395 Page Mill Rd., Palo Alto, CA, USA, 94306

10 Conclusions and Recommendations

A major advantage of employing an array of nanoelectrode ensembles is the selectivity for high priority analytes that can be realized by chemical modification of the nanoelectrode surfaces. Individual nanoelectrode elements within an array can be chemically treated to provide a working electrode surface with enhanced specificity and sensitivity for priority analytes processes that permit measurements of Pb^{2+}, As^{3+} and As^{5+} ionic species in water sources. Further selectivity in the analysis, including discrimination from interfering species in the water, can be derived from the fact that the thermodynamics and kinetics of the heterogeneous electron transfer reaction (i.e., the reduction or oxidation of the analyte) are different from those of many interferents. The deposition of gold surfaces in the nanoelectrode arrays provides a working electrode surface that is extremely well-suited to the analysis of As(III), As(V), Hg(II), Hg_xCl_y (so-called "reactive mercury), Cr(III), Cr(VI), and other priority analytes. Chemical modification of the nanoelectrode surfaces with polymeric coatings can increase the selectivity and sensitivity of some analyses via preferential adsorption of the analyte in the coating. For example, modification of carbon electrodes with amide-functionalized humic acids has been reported to produce a highly selective working electrode that can analyze mercury in river water at concentrations as low as 10 ppb.

In 18 months we moved from a concept of nanoelectrodes to a working prototype, complete with a nanoelectrode array of $9x10^7$ electrodes/cm^2, a sampling head that holds the water solution while making electrical contact to the array, a high-speed Potentiostat, an analytical protocol for trace detection, and development of supporting software, into a complete electrochemical field system. The focus of this project required the development and engineering of nanoelectrodes that permit measurement of electroactive species in high-resistivity water, i.e., without adding chemicals to increase conductivity. In our standard cell configuration where a counter electrode is place far from the working (nano) electrodes, our analysis required lower-than-standard additions of conductive salts, but in analysis using the "sandwich" nanoelectrode design, the ohmic drop between electrodes was extremely minute allowing analysis without conductive salts. Most of our standardizing for an analytical protocol first involved the use of commercial electrodes with the same geometric area as our nano electrode arrays. This work progressed to the nano electrode arrays for both the 1.4 and 10 μm spaced electrodes. The biggest engineering problem we had using these arrays was the PMMA polymer insulator film which swelled and delaminated during some of the study. Selecting PMMA as the insulating layer was based on its nature as a lithographic material that would permit pattern processing. To engineer more reliability and continued use into the arrays, the insulator should be pattern from a robust oxide that would allow physical polishing or cleaning at high potentials that impacted the weakly adherent polymers films. Chemically functionalized films would require replacement after fowling or stripping and reapplying a fresh film.

11 Appendix A

```
/* Nanoelectrode firmware ver 3.8
        PIC code for communicating with PIC controller board.
        anr&kbp 09-07-04
*/

//_____________________________COMPILER DIRECTIVES_____________________

#include "c:\nanoelec_stuff\16c62b.h"
#fuses HS, NOWDT, NOPROTECT, PUT, BROWNOUT
#use delay (clock=20000000, RESTART_WDT)
#use fast_io(A)
#use fast_io(B)

//_____________________________ System definitions_____________________

//_____________________________PORTA definitions_____________________

#define CS6   40              //Schematic label is ADG431 S2A
#define CS7    41        //Schematic label is ADG431 S2C
#define CS8     42            //Schematic label is MAX 187 CHIP SELECT
#define CS9           43              //Schematic label is LF398 HOLD LINE
#define CS10  44              //Schematic label is ADG431 S1B
#define CS11  45              //Schematic label is ADG431 S1C

//_____________________________PORTB definitions_____________________

#define SCLK  49              //Schematic label is SCLK
#define DOUT  50              //Schematic label is DOUT
#define CS1     51            //Schematic label is MAX5541_1 CHIP SELECT
#define CS2   52              //Schematic label is MAX5541_2 CHIP SELECT
#define CS3   53              //Schematic label is ADG431 S1C
#define CS4     54            //Schematic label is ADG431 S1D
#define CS5     55            //Schematic label is ADG431 S2B&D

//_____________________________PORTC definitions_____________________

#define TX    61   //Schematic label is TX
#define RX    60   //Schematic label is RX
#define CS12  56              //Schematic label is ADG431 S1A


//_____________________________VARIABLES_____________________
//DECLARES THESE AS GLOBAL
int msb1, lsb1, msb2, lsb2, tlsb1, tlsb2, tmsb1, tmsb2, vlsb1, vlsb2, counter;
int tmsb3, tlsb3, vmsb1, vmsb2, nlsb, nmsb;
int delta_vmsb, delta_vlsb;
long int delta_v;             //DECLARES THESE AS GLOBAL
long int Time1, Time2, Time3;
char datach[4], ch3[3];
//_____________________________PROTOTYPES_____________________
```

```
void set_DA1(int MSB, int LSB);
void set_DA2(int MSB, int LSB);
void read_VOC( void );
void read_VINT1( void );
void read_VINT2( void );
void flash_line(int n);
void sample_VOC(void);
void pulse_train_us(void);
void pulse_train_ms(void);
void Clear_Integrator(void);
void decode(void);
void delay_us_long_int(long int delay_time);
void calibration_1(void);
void calibration_2(void);
void Cyclic_VGrahamV1(void);
void Cyclic_VGrahamV2(void);
int  Convert_to_Hex(char ch1, ch2);
void long_sub1(void);
void long_add1(void);
void long_sub2(void);
void long_add2(void);

//_____RS232 Setup_____
#use rs232(baud=9600, xmit=TX, rcv=RX)

//_____MAIN_____

// Main program (startup)
void main( void )
{
msb1 = 0x00;
lsb1 = 0x00;
msb2 = 0x00;
lsb2 = 0x00;
tlsb1 = 0x0a;
tlsb2 = 0x0a;
tlsb3 = 0x0a;
tmsb1 = 0x00;
tmsb2 = 0x00;
tmsb3 = 0x00;
vlsb1 = 0x25;
vlsb2 = 0x53;
vmsb1 = 0x85;
vmsb2 = 0x85;
nlsb = 0x01;
nmsb = 0x00;
Time1=0x0a;
Time2=0x0a;
Time3=0x0a;
delta_v=0x006c;
output_b(0x7f);
output_a(0xf7);
output_c(0x01);
set_da1( msb1 , lsb1 );
set_da2( msb2 , lsb2 );
//  printf ("Hello World\n\r");
```

```
while(true)
  {


    ch3[0] = getch();
    if(ch3[0]=='^') decode();
    restart_wdt();



  //output_low(cs5);

  }
} //main()
//_____READ_VOC_____

//READS VALUE OF MAXIM 187 A/D CONVERTER

void read_VOC(VOID)
{
  int i3;
  msb1=0;
  lsb1=0;
  set_tris_a(0X00);
  OUTPUT_HIGH(CS8);
  set_tris_b(0X04);
  port_b_pullups(true);
  OUTPUT_HIGH(CS10);   //Open VINT1 switch
  OUTPUT_HIGH(CS11);   //Open VINT2 switch
  OUTPUT_LOW(CS12);    //Close VOC switch
  OUTPUT_LOW(SCLK);
  OUTPUT_HIGH(CS1);    //tristate the D/A converter
  OUTPUT_HIGH(CS2);    //tristate the D/A converter
  OUTPUT_HIGH(SCLK);
  OUTPUT_LOW(SCLK);
  OUTPUT_LOW(CS8);      //BEGIN CONVERSION
  restart_wdt();
  WHILE(!(INPUT(DOUT)));  //CHECK FOR END OF CONVERSION
  OUTPUT_HIGH(SCLK);
  OUTPUT_LOW(SCLK);     //BRINGS UP FIRST BIT
  FOR (i3=0; i3<=7; i3++)
  {
   MSB1=MSB1<<1;
   if (input(dout)) MSB1=MSB1+1;
   OUTPUT_HIGH(SCLK);
   OUTPUT_LOW(SCLK);
  }

   FOR (i3=0; i3<=7; i3++)
  {
   LSB1=LSB1<<1;
   if (input(dout)) LSB1=LSB1+1;
   OUTPUT_HIGH(SCLK);
   OUTPUT_LOW(SCLK);
  }
```

```
  OUTPUT_HIGH(CS8);   //end conversion
  OUTPUT_HIGH(CS12);  //open VOC switch
  // printf("%X%X\n\r",msb1,lsb1);

} //read_VOC()

//_____________________________________READ_VINT1_____________________________________

//READS VALUE OF MAXIM 187 A/D CONVERTER

void read_VINT1(VOID)
{
  int i3;
  msb1=0;
  lsb1=0;
  set_tris_a(0X00);
  OUTPUT_HIGH(CS8);
  set_tris_b(0X04);
  port_b_pullups(true);
  OUTPUT_HIGH(CS12);  //Open VOC switch
  OUTPUT_HIGH(CS11);  //Open VINT2 switch
  OUTPUT_LOW(CS10);   //Close VINT1 switch
  OUTPUT_LOW(SCLK);
  OUTPUT_HIGH(CS1);   //tristate the D/A converter
  OUTPUT_HIGH(CS2);   //tristate the D/A converter
  OUTPUT_HIGH(SCLK);
  OUTPUT_LOW(SCLK);
  OUTPUT_LOW(CS8);      //BEGIN CONVERSION
  restart_wdt();
  WHILE(!(INPUT(DOUT))); //CHECK FOR END OF CONVERSION
  OUTPUT_HIGH(SCLK);
  OUTPUT_LOW(SCLK);     //BRINGS UP FIRST BIT
  FOR (i3=0; i3<=7; i3++)
  {
   MSB1=MSB1<<1;
   if (input(dout)) MSB1=MSB1+1;
   OUTPUT_HIGH(SCLK);
   OUTPUT_LOW(SCLK);
  }
   FOR (i3=0; i3<=7; i3++)
  {
   LSB1=LSB1<<1;
   if (input(dout)) LSB1=LSB1+1;
   OUTPUT_HIGH(SCLK);
   OUTPUT_LOW(SCLK);
  }

  OUTPUT_HIGH(CS8);   //end conversion
  OUTPUT_HIGH(CS10);  //open VINT1 switch
  // printf("%X%X\n\r",msb1,lsb1);

} //read_INT1()

//_____________________________________READ_VINT1_____________________________________
```

```
//READS VALUE OF MAXIM 187 A/D CONVERTER

void read_VINT2(VOID)
{
  int i3;
  msb1=0;
  lsb1=0;
  set_tris_a(0X00);
  OUTPUT_HIGH(CS8);
  set_tris_b(0X04);
  port_b_pullups(true);
  OUTPUT_HIGH(CS12);  //Open VOC switch
  OUTPUT_HIGH(CS10);  //Open VINT1 switch
  OUTPUT_LOW(CS11);   //Close VINT2 switch
  OUTPUT_LOW(SCLK);
  OUTPUT_HIGH(CS1);   //tristate the D/A converter
  OUTPUT_HIGH(CS2);   //tristate the D/A converter

  OUTPUT_HIGH(SCLK);
  OUTPUT_LOW(SCLK);
  OUTPUT_LOW(CS8);      //BEGIN CONVERSION
  restart_wdt();
  WHILE(!(INPUT(DOUT)));  //CHECK FOR END OF CONVERSION
  OUTPUT_HIGH(SCLK);
  OUTPUT_LOW(SCLK);     //BRINGS UP FIRST BIT
  FOR (i3=0; i3<=7; i3++)
  {
   MSB1=MSB1<<1;
   if (input(dout)) MSB1=MSB1+1;
   OUTPUT_HIGH(SCLK);
   OUTPUT_LOW(SCLK);
  }
   FOR (i3=0; i3<=7; i3++)
  {
   LSB1=LSB1<<1;
   if (input(dout)) LSB1=LSB1+1;
   OUTPUT_HIGH(SCLK);
   OUTPUT_LOW(SCLK);
  }

  OUTPUT_HIGH(CS8);   //end conversion
  OUTPUT_HIGH(CS11);  //open VINT1 switch
  //  printf("%X%X\n\r",msb1,lsb1);

} //read_INT2()

//_____________________________________set_DA1_____________________________________

//SETS VALUE OF MAXIM 5541 D/A CONVERTER

void set_DA1(int msb, int lsb)
{
  int i1;
  SET_TRIS_A(0X00);
  OUTPUT_HIGH(CS8);                  //Tristate A/D converter
  SET_TRIS_B(0X00);
```

```
  port_b_pullups(true);
  OUTPUT_HIGH(CS1);
  OUTPUT_LOW(SCLK);
  OUTPUT_LOW(CS1);
  FOR (i1=0; i1<8; i1++)
  {
   if ( MSB & 0x80 )
   {
    OUTPUT_HIGH(DOUT);
   }
   ELSE
   {
    OUTPUT_LOW(DOUT);
   }

   MSB=MSB<<1;
   OUTPUT_HIGH(SCLK);
   OUTPUT_LOW(SCLK);

  }
   FOR (i1=0; i1<8; i1++)
  {
   if ( LSB & 0x80 )
   {
    OUTPUT_HIGH(DOUT);
   }
   ELSE
   {
    OUTPUT_LOW(DOUT);
   }
   LSB=LSB<<1;
   OUTPUT_HIGH(SCLK);
   OUTPUT_LOW(SCLK);
  }
  OUTPUT_HIGH(CS1);
} //set_DA1()

//_____________________________________set_DA2_____________________________________

//SETS VALUE OF MAXIM 5541 D/A CONVERTER

void set_DA2(int msb, int lsb)
{
  int i2;
  SET_TRIS_A(0X00);
  OUTPUT_HIGH(CS8);                    //Tristate A/D converter
  SET_TRIS_B(0X00);
  port_b_pullups(true);
  OUTPUT_HIGH(CS2);
  OUTPUT_LOW(SCLK);
  OUTPUT_LOW(CS2);
  FOR (i2=0; i2<8; i2++)
  {
   if ( MSB & 0x80 )
   {
    OUTPUT_HIGH(DOUT);
```

```
    }
    ELSE
    {
      OUTPUT_LOW(DOUT);
    }

    MSB=MSB<<1;
    OUTPUT_HIGH(SCLK);
    OUTPUT_LOW(SCLK);

   }
    FOR (i2=0; i2<8; i2++)
   {
    if ( LSB & 0x80 )
    {
      OUTPUT_HIGH(DOUT);
    }
    ELSE
    {
      OUTPUT_LOW(DOUT);
    }
    LSB=LSB<<1;
    OUTPUT_HIGH(SCLK);
    OUTPUT_LOW(SCLK);
   }
   OUTPUT_HIGH(CS2);
} //set_DA2()

//_____Flash_line(n)_____

void flash_line(int n)
{
  int i;
  for (i=0; i<n; i++)
   {
     output_high( cs7 );
     output_low( cs7 );

   }
 } //flash_line()


 //_____Calibration_1_____

void Calibration_1(void)
{
  int i;
  long int Temp_v;
   for(i=0; i<115; i++)
   {
      output_high(cs4);          //open V2 switch
      output_high(cs6);          //open VOC switch
      output_low(cs3);           //close V1 switch
      delay_ms(Time1);
      output_high(cs3);          //open V1 switch
```

```
    output_low(cs4);                //close V2 switch
    delay_ms(Time2);
    output_high(cs4);               //open V2 switch
    output_low(cs6);                //close VOC
    delay_ms(Time3);

    Temp_v = make16(vmsb1,vlsb1);
    Temp_v = Temp_v - delta_v;
    vlsb1 = (int) (Temp_v & 0x00ff);
    vmsb1 = (int) (Temp_v >> 8);          //Change V1

    Temp_v = make16(vmsb2,vlsb2);
    Temp_v = Temp_v - delta_v;
    vlsb2 = (int) (Temp_v & 0x00ff);
    vmsb2 = (int) (Temp_v >> 8);          //Change V2

    set_DA1(vmsb1, vlsb1);          //Update D/A1
    set_DA2(vmsb2, vlsb2);          //Update D/A2
    //printf("V1=%X%X dV=%x\n\r",vmsb1,vlsb1,delta_v);
    //printf("V2=%X%X dV=%x\n\r",vmsb2,vlsb2,delta_v);
   }
 } //Calibration_1()

//_____________________________________Calibration_2_____________________________________

void Calibration_2(void)
{
  int i, vlsb11, vmsb11;
  long int Temp_v1, Temp_v2;

    Time2=0x00;                     //make time delay for 2 and 3 zero
    Time3=0x00;
    output_high(cs4);               //open V2 switch
    output_high(cs6);               //open VOC switch
    output_low(cs3);                //close V1 switch
    Temp_v1 = make16(vmsb1,vlsb1);
    Temp_v2 = make16(vmsb2,vlsb2) + delta_v;

    //printf("1 V1=%X  V2=%X dV=%x\n\r",Temp_v1, Temp_v2 ,delta_v);

  while ( Temp_v1 > Temp_v2)
  {
    delay_ms(Time1);
    Temp_v1 = Temp_v1 - delta_v;
    vlsb11 = (int) (Temp_v1 & 0x00ff);
    vmsb11 = (int) (Temp_v1 >> 8);          //Change V1
    set_DA1(vmsb11, vlsb11);          //Update D/A1

    //printf("2 Vmsb=%X  Vlsb=%X dV=%x\n\r",vmsb11, vlsb11 ,delta_v);

   }

    Temp_v2 = make16(vmsb1,vlsb1) - delta_v;
    Temp_v1 = make16(vmsb2,vlsb2);
  while ( Temp_v1 < Temp_v2)
  {
```

```
    delay_ms(Time1);
    Temp_v1 = Temp_v1 + delta_v;
    vlsb11 = (int) (Temp_v1 & 0x00ff);
    vmsb11 = (int) (Temp_v1 >> 8);          //Change V1
    set_DA1(vmsb11, vlsb11);          //Update D/A1

    //printf("3 Vmsb=%X  Vlsb=%X dV=%x\n\r",vmsb11, vlsb11 ,delta_v);

    Time2=0x0a;                 //make time delay for 2 and 3 default
    Time3=0x0a;
  }
} //Calibration_1()

//_____________________________________Cyclic_VGrahamV1_____________________________

void Cyclic_VGrahamV1(void)
{
    output_high(cs4);             //open V2 switch
    output_high(cs6);             //open VOC switch
    output_high(cs3);             //open V1 switch
    set_DA1(vmsb1, vlsb1);          //Update D/A1
    output_low(cs3);              //close V1 switch
    delay_us(100);
    output_low(cs5);              //expose Cell


} //Cyclic_VGrahamV1()

//_____________________________________Cyclic_VGrahamV2_____________________________

void Cyclic_VGrahamV2(void)
{
    output_high(cs3);             //open V1 switch
    output_high(cs6);             //open VOC switch
    output_high(cs4);             //open V2 switch
    set_DA2(vmsb2, vlsb2);          //Update D/A2
    output_low(cs4);              //close V2 switch
    delay_us(100);
    output_low(cs5);              //expose Cell


} //Cyclic_VGrahamV2()



//_____________________________________sample_VOC(void)_____________________________
void sample_VOC(void)
{

  output_high(cs5);               //isolate cell
  delay_us(50);
  output_high(cs9);               //Sample LF398
  delay_ms(5);
  output_low(cs9);                //Hold LF398

 //output_low(cs5);
```

```
}// sample_VOC()

//_____pulse_train_us_____
void pulse_train_us(void)

{
  int i;
  for(i=0; i<nlsb; i++)
  {
    output_high(cs6);          //open VOC switch
    output_high(cs4);          //open V2 switch
    output_low(cs5);           //expose cell to drive
    delay_us(10);
    output_low(cs3);           //close V1 switch
    delay_us(Time1);
    output_high(cs3);          //open V1 switch
    output_low(cs4);           //close V2 switch
    delay_us(Time2);
    output_high(cs4);          //open V2 switch
   //output_low(cs6);          //close VOC
    delay_us(Time3);
    output_high(cs5);          //isolate cell from drive
    output_low(cs6);           //place VOC on J3
  }
}// pulse_train()

//_____pulse_train_ms_____
void pulse_train_ms(void)

{
  int i;
  for(i=0; i<nlsb; i++)
  {
    output_high(cs6);          //open VOC switch
    output_high(cs4);          //open V2 switch
    output_low(cs5);           //expose cell to drive
    delay_us(10);
    output_low(cs3);           //close V1 switch
    delay_ms(Time1);
    output_high(cs3);          //open V1 switch
    output_low(cs4);           //close V2 switch
    delay_ms(Time2);
    output_high(cs4);          //open V2 switch
   //output_low(cs6);          //close VOC
    delay_ms(Time3);
    output_high(cs5);          //isolate cell from drive
    output_low(cs6);           //place VOC on J3
  }
}// pulse_train()
//_____pulse_train_long_____
void pulse_train_long(void)

{
  int i;
  for(i=0; i<nlsb; i++)
  {
```

```
    output_high(cs6);              //open VOC switch
    output_high(cs4);              //open V2 switch
    output_low(cs5);               //expose cell to drive
    delay_us(10);
    output_low(cs3);               //close V1 switch
    delay_us_long_int(Time1);
    output_high(cs3);              //open V1 switch
    output_low(cs4);               //close V2 switch
    delay_us_long_int(Time2);
    output_high(cs4);              //open V2 switch
   //output_low(cs6);              //close VOC
    delay_us_long_int(Time3);
    output_high(cs5);              //isolate cell from drive
    output_low(cs6);               //place VOC on J3
  }
}// pulse_train_long()


//_____________________________________delay_us_long_int_____________________________________

void delay_us_long_int(long int delay_time)
{
  int time1;
  time1= (int) (delay_time & 0x00ff);
  delay_us(time1);
  time1 = (int) (delay_time>>8);
  while (time1 > 0)
    {
      delay_us(0xff);
      time1=time1-1;
    };

}//delay_us_long_int

//_____________________________________Clear Integrator_____________________________________
void Clear_Integrator(void)
{
  output_low(cs7);
  delay_us(100);
  output_high(cs7);

}// Clear_Integrator()

//_____________________________________Decode_____________________________________
void decode(void)
{
  int val;
 // printf ("Decode Subroutine\n\r");
  setup_wdt(wdt_2304ms);
  ch3[1] = getch();
  restart_wdt();

 // printf ("ch3[1]=%c\n\r",ch3[1]);
  ch3[2] = getch();
  restart_wdt();
 // printf ("ch3[2]=%c\n\r",ch3[2]);
```

```
val=ch3[1]+ch3[2];

switch (val)
{
  case 't'+'1':

    datach[0] = getch();
    restart_wdt();
    datach[1] = getch();
    restart_wdt();
    datach[2] = getch();
    restart_wdt();
    datach[3] = getch();
    setup_wdt(wdt_288ms);
    tmsb1=Convert_to_Hex(datach[0],datach[1]);
    tlsb1=Convert_to_Hex(datach[2],datach[3]);
    Time1=((long) tmsb1<<8) + (long) tlsb1;
    //printf("%x\n\r",Time1);
    break;

   case 't'+'2':

    datach[0] = getch();
    restart_wdt();
    datach[1] = getch();
    restart_wdt();
    datach[2] = getch();
    restart_wdt();
    datach[3] = getch();
    setup_wdt(wdt_288ms);
    tmsb2=Convert_to_Hex(datach[0],datach[1]);
    tlsb2=Convert_to_Hex(datach[2],datach[3]);
    Time2=((long) tmsb2<<8) + (long) tlsb2;
    // printf("%x\n\r",Time2);
    break;

   case 't'+'3':

    datach[0] = getch();
    restart_wdt();
    datach[1] = getch();
    restart_wdt();
    datach[2] = getch();
    restart_wdt();
    datach[3] = getch();
    setup_wdt(wdt_288ms);
    tmsb3=Convert_to_Hex(datach[0],datach[1]);
    tlsb3=Convert_to_Hex(datach[2],datach[3]);
    Time3=((long) tmsb3<<8) + (long) tlsb3;
    // printf("%x\n\r",Time3);
    break;

   case 'V'+'1':

    datach[0] = getch();
    restart_wdt();
```

```
  datach[1] = getch();
  restart_wdt();
  datach[2] = getch();
  restart_wdt();
  datach[3] = getch();
  setup_wdt(wdt_288ms);
  vmsb1=Convert_to_Hex(datach[0],datach[1]);
  vlsb1=Convert_to_Hex(datach[2],datach[3]);
  break;

case 'V'+'2':

  datach[0] = getch();
  restart_wdt();
  datach[1] = getch();
  restart_wdt();
  datach[2] = getch();
  restart_wdt();
  datach[3] = getch();
  setup_wdt(wdt_288ms);
  vmsb2=Convert_to_Hex(datach[0],datach[1]);
  vlsb2=Convert_to_Hex(datach[2],datach[3]);
  break;

case 'V'+'C':
   sample_VOC();
  break;

 case 'D'+'V':

  datach[0] = getch();
  restart_wdt();
  datach[1] = getch();
  restart_wdt();
  datach[2] = getch();
  restart_wdt();
  datach[3] = getch();
  setup_wdt(wdt_288ms);
  delta_vmsb=Convert_to_Hex(datach[0],datach[1]);
  delta_vlsb=Convert_to_Hex(datach[2],datach[3]);
  delta_v = make16(delta_vmsb,delta_vlsb);
  break;

case 'D'+'1':

  msb1 = 0x00;
  lsb1 = 0x00;
  msb2 = 0x00;
  lsb2 = 0x00;
  tlsb1 = 0x0a;
  tlsb2 = 0x0a;
  tmsb1 = 0x00;
  tmsb2 = 0x00;
  Time1 = 0x0a;
  Time2 = 0x0a;
  Time3 = 0x0a;
```

```
  vlsb1 = 0x25;
  vlsb2 = 0x53;
  vmsb1 = 0x85;
  vmsb2 = 0x85;
  nlsb = 0x01;
  nmsb = 0x00;
  output_b(0x7f);
  output_a(0xf7);
  set_da1( msb1 , lsb1 );
  set_da2( msb2 , lsb2 );
  break;

 case 'n'+'1':

  datach[0] = getch();
  restart_wdt();
  datach[1] = getch();
  restart_wdt();
  datach[2] = getch();
  restart_wdt();
  datach[3] = getch();
  setup_wdt(wdt_288ms);
 // printf("Hex value = 4%c\n\r",datach[0],datach[1],datach[2],datach[3]);
  nmsb=Convert_to_Hex(datach[0],datach[1]);
  nlsb=Convert_to_Hex(datach[2],datach[3]);
  break;

case 'm'+'v':

  read_VOC();
  printf("%x%x\n\r",msb1,lsb1);
  break;

case 'm'+'x':

  read_VINT1();
  printf("%x%x\n\r",msb1,lsb1);
  break;


case 'm'+'y':

  read_VINT2();
  printf("%x%x\n\r",msb1,lsb1);
  break;

case 'i'+'t':
   set_DA1(VMSB1, VLSB1);
   set_DA2(VMSB2, VLSB2);
   sample_VOC();
   Clear_Integrator();
  break;

case 't'+'u':

  //Clear_Integrator();
```

```
      pulse_train_us();

      break;
    case 't'+'m':

      //Clear_Integrator();
      pulse_train_ms();

      break;

    case 't'+'z':

      //Clear_Integrator();
      pulse_train_long();

      break;

    case 'n'+'^':

      while(true)
      {
      pulse_train_us();
      sample_VOC();
      }

      break;

    case 'P'+'R':
      printf ("%x%x %x%x %x%x %x%x %x%x %x%x %x%x\n\r", tmsb1, tlsb1, tmsb2, tlsb2,
tmsb3, tlsb3, vmsb1, vlsb1, vmsb2, vlsb2, nmsb, nlsb, delta_vmsb, delta_vlsb);


      break;

    case 'c'+'1':
      calibration_1();
      break;

    case 'c'+'2':
      calibration_2();
      break;

    case 'c'+'v':
      Cyclic_VGrahamV1();
      break;

    case 'c'+'x':
      Cyclic_VGrahamV2();
      break;

    case 'o'+'1':
      output_high(cs5);
      break;

    case 'o'+'2':
      output_low(cs5);
```

```
        break;

      default:

       // printf("^default subroutine\n\r");
        break;
    }
} //decode()

//_____Convert_to_Hex_____
int Convert_to_Hex(char ch1, ch2)

{
    int val1;
    val1=0;
        // printf("Convert_to_Hex val1 %x %c %c\n\r",val1,ch1,ch2);
    switch(ch1)
      {
        case '0':
          val1=0x00;
          break;
        case '1':
          val1=0x10;
          break;
        case '2':
          val1=0x20;
          break;
        case '3':
          val1=0x30;
          break;
        case '4':
          val1=0x40;
          break;
        case '5':
          val1=0x50;
          break;
        case '6':
          val1=0x60;
          break;
        case '7':
          val1=0x70;
          break;
        case '8':
          val1=0x80;
          break;
        case '9':
          val1=0x90;
          break;
        case 'a':
          val1=0xa0;
          break;
        case 'b':
          val1=0xb0;
          break;
        case 'c':
          val1=0xc0;
```

```
      break;
    case 'd':
      val1=0xd0;
      break;
    case 'e':
      val1=0xe0;
      break;
    case 'f':
      val1=0xf0;
      break;
    default:;
}
    // printf("Convert_to_Hex MSB %x\n\r",val1);
      switch(ch2)
{
    case '0':
      val1=val1|0x00;
      break;

    case '1':
      val1=val1|0x01;
      break;
    case '2':
      val1=val1|0x02;
      break;
    case '3':
      val1=val1|0x03;
      break;
    case '4':
      val1=val1|0x04;
      break;
    case '5':
      val1=val1|0x05;
      break;
    case '6':
      val1=val1|0x06;
      break;
    case '7':
      val1=val1|0x07;
      break;
    case '8':
      val1=val1|0x08;
      break;
    case '9':
      val1=val1|0x09;
      break;
    case 'a':
      val1=val1|0x0a;
      break;
    case 'b':
      val1=val1|0x0b;
      break;
    case 'c':
      val1=val1|0x0c;
      break;
    case 'd':
```

```
            val1=val1|0x0d;
            break;
          case 'e':
            val1=val1|0x0e;
            break;
          case 'f':
            val1=val1|0x0f;
            break;
          default:;
        }
      // printf("Convert_to_Hex LSB %x\n\r",val1);
      return val1;

} //Convert_to_Hex
```

12 Appendix B

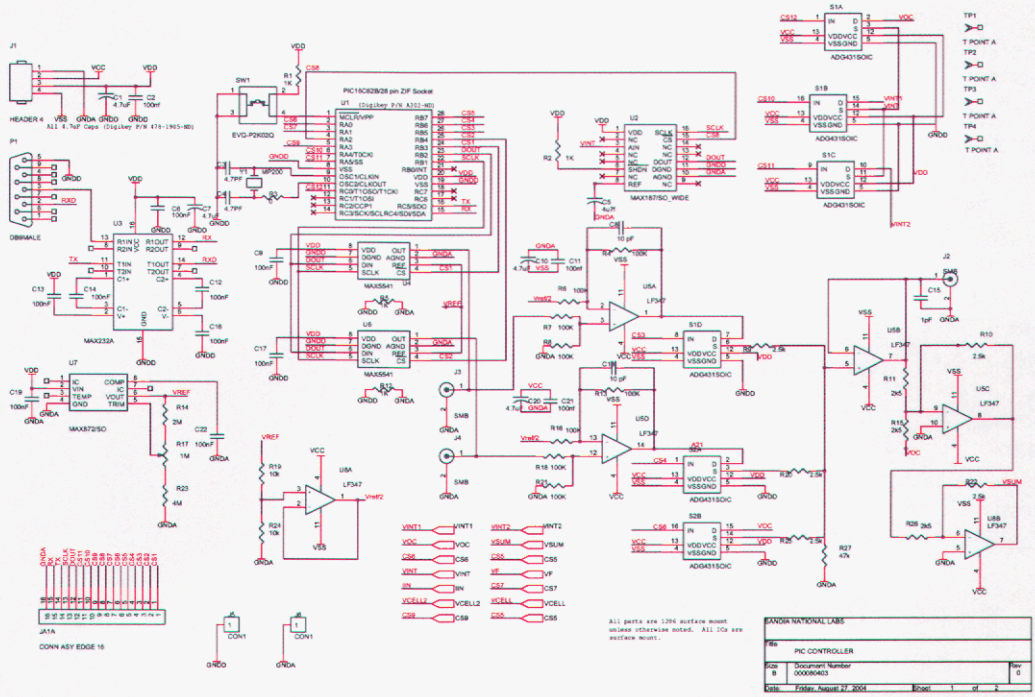

Figure. 12.1: Signal generation section of potentiostat.

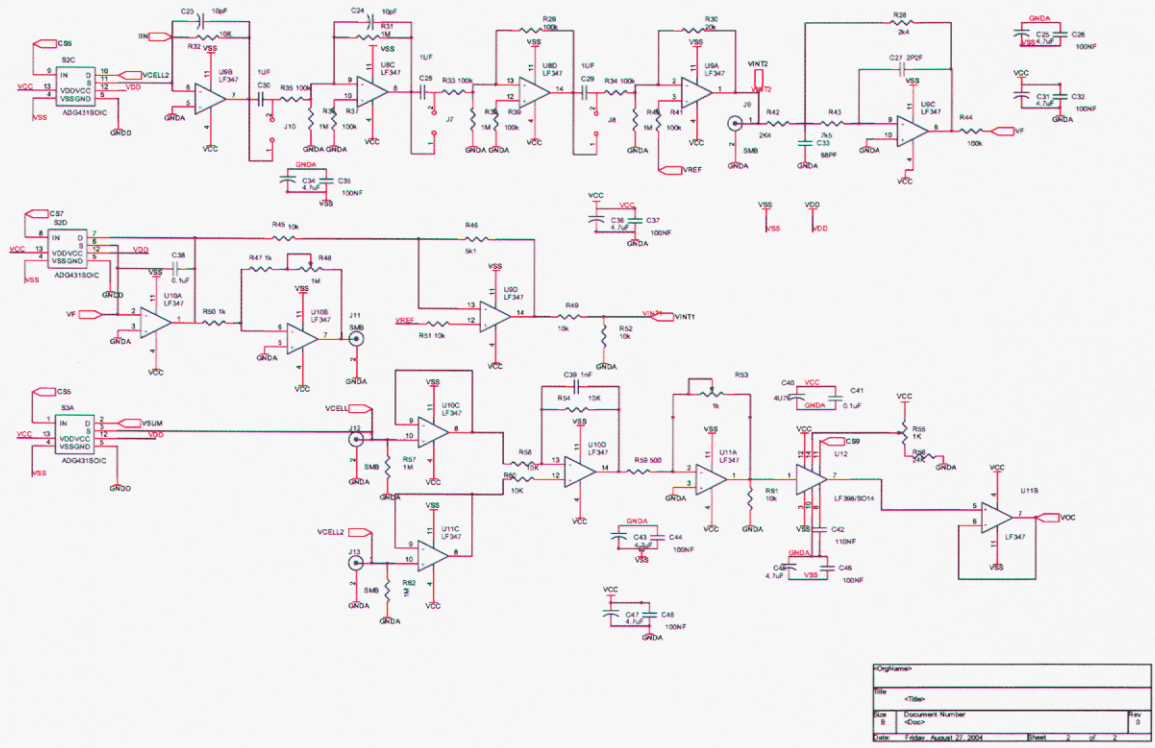

Figure 12.2: Transimpedance amplifier and open circuit voltage measurement circuits.

13 Distribution

5	MS	1425	W. G. Yelton,	01743
3		1425	K. B. Pfeifer,	01744
1		1425	N. J. Gurule,	01743
1		0958	M. J. Kelly,	14253
1		0161	C. I. Ashby,	11500
1		0734	W. Einfeld,	06245
1		0750	M. D. Siegel,	06118
1		0750	T. E. Hinkebein,	06118
1		1425	S. A. Casalnuovo,	01744
1		0603	J. J. Hudgens,	01743
1		0892	D. R. Wheeler,	01764
1		1080	C. D. James,	01769
1		1077	T. J. Zipperian,	01740
1		1080	S. S. Mani,	01749
1		1425	J. H. Flemming,	01744
1		0892	S. M. Brozik,	01744
1		1413	B. C. Bunker,	01116
1		9018	Central Technical Files,	08945-1
2		0899	Technical Library,	09616
1		0161	Patent and Licensing Office,	11500
1		0123	Donna Chavez	1001